REPORT DOCUMENTATION PAGE

Form Approved OMB NO. 0704-0188

The public reporting burden for this collection of information is estimated to average 1 hour per response, including the time for reviewing instructions, searching existing data sources, gathering and maintaining the data needed, and completing and reviewing the collection of information. Send comments regarding this burden estimate or any other aspect of this collection of information, including suggesstions for reducing this burden, to Washington Headquarters Services, Directorate for Information Operations and Reports, 1215 Jefferson Davis Highway, Suite 1204, Arlington VA, 22202-4302. Respondents should be aware that notwithstanding any other provision of law, no person shall be subject to any oenalty for failing to comply with a collection of information if it does not display a currently valid OMB control number.
PLEASE DO NOT RETURN YOUR FORM TO THE ABOVE ADDRESS.

1. REPORT DATE (DD-MM-YYYY)	2. REPORT TYPE	3. DATES COVERED (From - To)
13-06-2018	Final Report	2-Jun-2015 - 1-Jun-2018

4. TITLE AND SUBTITLE
Final Report: Globally Convergent Inverse Algorithms via Carleman Weight Functions: Theory, Numerical Studies and Experimental Verifications

5a. CONTRACT NUMBER
W911NF-15-1-0233

5b. GRANT NUMBER

5c. PROGRAM ELEMENT NUMBER
611102

6. AUTHORS

5d. PROJECT NUMBER

5e. TASK NUMBER

5f. WORK UNIT NUMBER

7. PERFORMING ORGANIZATION NAMES AND ADDRESSES
University of North Carolina - Charlotte
9201 University City Boulevard

Charlotte, NC 28223 -0001

8. PERFORMING ORGANIZATION REPORT NUMBER

9. SPONSORING/MONITORING AGENCY NAME(S) AND ADDRESS (ES)
U.S. Army Research Office
P.O. Box 12211
Research Triangle Park, NC 27709-2211

10. SPONSOR/MONITOR'S ACRONYM(S)
ARO

11. SPONSOR/MONITOR'S REPORT NUMBER(S)
65549-MA.34

12. DISTRIBUTION AVAILIBILITY STATEMENT
Approved for public release; distribution is unlimited.

13. SUPPLEMENTARY NOTES
The views, opinions and/or findings contained in this report are those of the author(s) and should not contrued as an official Department of the Army position, policy or decision, unless so designated by other documentation.

14. ABSTRACT

15. SUBJECT TERMS

16. SECURITY CLASSIFICATION OF:			17. LIMITATION OF ABSTRACT	15. NUMBER OF PAGES	19a. NAME OF RESPONSIBLE PERSON
a. REPORT	b. ABSTRACT	c. THIS PAGE			Mikhail Klibanov
UU	UU	UU	UU		19b. TELEPHONE NUMBER 704-687-1373

RPPR Final Report
as of 15-Jun-2018

Agency Code:

Proposal Number: 65549MA **Agreement Number: W911NF-15-1-0233**
INVESTIGATOR(S):

Name: Ph.D Mikhail Klibanov
Email: mklibanv@uncc.edu
Phone Number: 7046871373
Principal: Y

Organization: **University of North Carolina - Charlotte**
Address: 9201 University City Boulevard, Charlotte, NC 282230001
Country: USA
DUNS Number: 066300096 EIN: 560791228
Report Date: 01-Sep-2018 Date Received: 13-Jun-2018
Final Report for Period Beginning 02-Jun-2015 and Ending 01-Jun-2018
Title: Globally Convergent Inverse Algorithms via Carleman Weight Functions: Theory, Numerical Studies and Experimental Verifications
Begin Performance Period: 02-Jun-2015 **End Performance Period:** 01-Jun-2018
Report Term: 0-Other
Submitted By: Ph.D Mikhail Klibanov Email: mklibanv@uncc.edu
Phone: (704) 687-1373
Distribution Statement: 1-Approved for public release; distribution is unlimited.

STEM Degrees: 0 **STEM Participants:** 0

Major Goals: This project has three major goals:

Goal 1. The analytical development and numerical implementation of the so-called "tail functions" method globally convergent numerical method in the frequency domain for Coefficient Inverse Scattering Problems (CISPs).

Goal 2. The analytical development and numerical implementation of the globally convergent numerical method for CISPs, which is based on the construction of weighted globally strictly convex Tikhonov-like functionals. The key element of such a functional is the presence of the Carleman Weight Function in it.

Goal 3. Analytical and numerical studies of Phaseless Coefficient Inverse Scattering Problems (CISPs).

The main application of Goals 1 and 2 is in STANDOFF imaging and identification of antipersonnel mine-like targets and improvised explosive devices (IEDs). This application is addressed via our work with a variety of microwave experimental data.

The main application of Goal 3 is in imaging of nanostructures and biological cells.

Accomplishments: The tail functions method globally convergent numerical method (GCM) was described in detail in the previous annual report of the PI which has covered the period of 06/01/16-05/31/17. In addition, the PI's team has mostly worked on the convexification method during this reportage period of 06/01/17-05/31/18. In fact, the convexification GCM is both more promising and more mathematically elegant than the tail functions GCM.

Thus the focus of the current annual report is on the convexification method. Recall that the main application of both GCMs of this project is in STANDOFF imaging and identification of antipersonnel land mines and IEDs.

Accomplishments under Goals in this reportage period are:

1. The PI got a prestigious award. In August 2017, Sobolev Institute of Mathematics has awarded the PI Golden Medal for "Distinguished Impact in Mathematics". Publications on the topic of Phaseless Inverse Scattering Problems, sponsored by this grant, have played a major impact in the award decision. This is a life time achievement of the PI. Other awardees of this Golden Medal are World famous mathematicians, including one

Fields Laureate (E.I. Zelmanov).

2. In the case of a single direction of the incident plane wave, the theory of the convexification GCM is fully developed.

3. Furthermore, the convexification method of item 2 was successfully tested on the most challenging case: the case of experimental backscattering data for buried mine-like and IED-like targets. It is demonstrated that the convexification computes very accurately both locations and dielectric constants of these targets. However, shapes are not computed well, see item 4.

4. To accurate compute shapes of targets as well, the PI has recently started to develop an extension of the convexification to the case when either the direction of the incident plane wave is changing or the point source is moving along a straight line. The first computational result shows promise. Nevertheless, many things in this direction still need to be clarified.

5. The classical and very popular inverse problem of Electrical Impedance Tomography (EIT) is solved numerically by the version of item 4 of the convexification method. This is the FIRST solution of this problem by a globally convergent numerical method.

6. The convexification method of item 2 was successfully tested on experimental data collected by engineers of ARL Drs. L. Nguyen and A. Sullivan. During this reportage period one (1) joint paper with Nguyen and Sullivan was published and one (1) was submitted for publication. In the period of 2012-2018 five (5) joint papers were published and one (1) was submitted.

7. Thus, a quite fruitful collaboration of the PI with engineers from ARL has been successfully ongoing since 2012.

8. Publications during the reportage period acknowledging the support of this grant: eight (8) papers are published and five (5) are submitted for publication. As to the entire period of this funding, 06/01/15-05/31/18, total twenty two (22) papers were published/submitted. All papers are in refereed journals.

9. Two numerical methods for Phaseless Coefficient Inverse Scattering Problem were developed. One of them was successfully tested on experimental data.

10. Publications of the PI with coauthors concerning Phaseless Coefficient Inverse Scattering Problem constitute the FIRST SOLUTION of a LONG STANDING problem posed by French mathematicians K. Chadan and P.C. Sabatier in 1977 in their well known book "Inverse Problems in Quantum Scattering Theory", Springer, 1977.

RPPR Final Report
as of 15-Jun-2018

Training Opportunities: During the reportage period of 2017-2018 two (2) postdoctoral research associates were trained and partially supported by this grant:

1. Dr. Aleksandr E. Kolesov

2. Dr. Nikolaj A. Koshev

However, during the entire funding period of 2015-2018 total five (5) postdoctoral research associates were trained and partially supported by this grant. Three additional persons are:

3. Dr. Loc Hoang Nguyen

4. Dr. Hui Liu

5. Dr. Dinh-Liem Nguyen.

The PI is proud to report that Drs. L.H. Nguyen and D.-L. Nguyen got tenure track assistant professors positions in US universities after working with the PI:

A. Dr. L.H. Nguyen got tenure track assistant professors position in Department of Mathematics and Statistics of University of North Carolina at Charlotte.

B. Dr. D.-L. Nguyen got tenure track assistant professors position in Department of Mathematics of Kansas State University.

Publications of trainees with the acknowledgment of the support of this grant:

1. Dr. A. E. Kolesov has published/submitted references [1,4,5,6,11,13] of the attached pdf file with the annual report; also see the same numbers of references in "Dissemination".

2. Dr. N.A. Koshev has submitted reference [10] of the attached pdf file of the annual report. This work was done during his one year appointment of 2017-2018.

3. Dr. L.H. Nguyen has published/submitted references [2,4,5,8,9,10,15,16] of the attached pdf file with the annual report; also see the same numbers of references in "Dissemination".

4. Dr. Hui Liu has published references [2,4] of the attached pdf file with the annual report; also see the same numbers of references in "Dissemination".

5. Dr. D.-L. Nguyen has published/submitted references [2,4,5,8,9,10,11] of the attached pdf file with the annual report; also see the same numbers of references in "Dissemination".

RPPR Final Report
as of 15-Jun-2018

Results Dissemination: Total nine (9) papers [1]-[9] were published during the reportage period of 2017-2018 and
five papers (5) [10]-[14] were submitted in this period.

Total twenty two (22) papers [1]-[22] were published/submitted during the period of this funding 06/01/15-05/31/18.

All papers [1]-[22] are in refereed journals and all these acknowledge the support of this grant.

These papers are listed below:

1. M.V. Klibanov and A.E. Kolesov, Convexification of a 3-D coefficient inverse scattering problem, Computers and Mathematics with Applications, available online of this journal, https://doi.org/10.1016/j.camwa.2018.03.016, 2018.

2. M. V. Klibanov, D.-L. Nguyen, L. H. Nguyen, and H. Liu, A globally convergent numerical method for a 3D coefficient inverse problem with a single measurement of multifrequency data, Inverse Problems and Imaging, 12, 493-523, 2018.

3. M.V. Klibanov and V.G. Romanov, Uniqueness of a 3-D coefficient inverse scattering problem without the phase information, Inverse Problems, 33, 095007, 2017.

4. D.-L. Nguyen, M. V. Klibanov, L.H. Nguyen, A. E. Kolesov, M. A. Fiddy and H. Liu, Numerical solution for a coefficient inverse problem with multi-frequency experimental raw data by a globally convergent algorithm, J. Computational Physics, 345, 17-32, 2017.

5. A. E. Kolesov, M. V. Klibanov, L. H. Nguyen, D.-L. Nguyen, and N. T. Thanh, Single measurement experimental data for an inverse medium problem inverted by a multifrequency globally convergent numerical method, Applied Numerical Mathematics, 120, 176-196, 2017.

6. M.V. Klibanov, A.E. Kolesov, L. Nguyen and A. Sullivan, Globally strictly convex cost functional for a 1-D inverse medium scattering problem with experimental data, SIAM J. Applied Mathematics, 77 1733-1755, 2017.

7. M. V. Klibanov, Convexification of restricted Dirichlet-to-Neumann map, J. Inverse and Ill-Posed Problems, 25, 669-685, 2017.

8. D.-L. Nguyen, M. V. Klibanov, L.H. Nguyen and M.A. Fiddy, Imaging of buried objects from multi-frequency experimental data using a globally convergent inversion method, Journal of Inverse and Ill-Posed Problems, published online of this journal, DOI: 10.1515/jiip-2017-0047, 2017.
9. M.V. Klibanov, A phaseless inverse scattering problem for the 3-D Helmholtz equation,
Inverse Problems and Imaging, 11, 263-276, 2017.

10. M.V. Klibanov, D.-L. Nguyen and L. H. Nguyen, A coefficient inverse problem with a single measurement of phaseless scattering data, submitted for publication, www.arxiv.org: 1710.04804, submitted for publication, 2018.

11. M.V. Klibanov, N.A. Koshev, D.-L. Nguyen, L. H. Nguyen, A. Brettin and V.N. Astratov, A numerical method to solve a phaseless coefficient inverse problem from a single measurement of experimental data, submitted for publication, available on www.arxiv.org: 1803.01374, submitted for publication, 2018.

12. M.V. Klibanov, A.E. Kolesov and D.-L. Nguyen, Convexification method for a coefficient inverse problem and its performance for experimental backscatter data for buried targets, available on www.arxiv.org: 1850.07618, 2018, submitted for publication.

13. M. V. Klibanov, J. Li and W. Zhang, Electrical impedance tomography with restricted Dirichlet-to-Neumann map data, available www.arxiv.org: 1803.11193, 2018, submitted for publication.

14. M.V. Klibanov, A.E. Kolesov, A. Sullivan and L. Nguyen, A new version of the convexification method for a 1-D

coefficient inverse problem with experimental data, available on www.arxiv.org: 1805.06025, 2018, submitted for publication.

15. M.V. Klibanov, L.H. Nguyen, A. Sullivan and L. Nguyen, A globally convergent numerical method for a 1-d inverse medium problem with experimental data, Inverse Problems and Imaging, 10, 1057-1085, 2016.

16. M.V. Klibanov, L.H. Nguyen and K. Pan, Nanostructures imaging via numerical solution of a 3-D inverse scattering problem without the phase information, Applied Numerical Mathematics, 110, 190-203, 2016.

17. A.B. Bakushinskii, M.V. Klibanov and N.A. Koshev, Carleman weight functions for a globally convergent numerical method for ill-posed Cauchy problems for some quasilinear PDEs, Nonlinear Analysis: Real World Applications, 34, 201-224, 2017.

18. M.V. Klibanov, N.A. Koshev, J. Li and A.G. Yagola, Numerical solution of an ill-posed Cauchy problem for a quasilinear parabolic equation using a Carleman weight function, J. Inverse and Ill-Posed Problems, 24, 761-776, 2016.

19. M.V. Klibanov and V.G. Romanov, The first solution of a long standing problem: Reconstruction formula for a 3-d phaseless inverse scattering problem for the Schrödinger equation, J. Inverse and Ill-Posed Problems, 23, 415-428, 2015.

20. M.V. Klibanov and V.G. Romanov, Reconstruction procedures for two inverse scattering problems without the phase information, SIAM J. Appl. Math., 76, 178-196, 2016.

21. M.V. Klibanov and V.G. Romanov, Two reconstruction procedures for a 3-D phaseless inverse scattering problem for the generalized Helmholtz equation, Inverse Problems, 32, 015005, 2016.

22. M.V. Klibanov, Carleman weight functions for solving ill-posed Cauchy problems for quasilinear PDEs, Inverse Problems, 31, 125007, 2015.

Honors and Awards: The PI got a prestigious award. In August 2017, Sobolev Institute of Mathematics has awarded the PI Golden Medal for "Distinguished Impact in Mathematics". Publications on the topic of Phaseless Inverse Scattering Problems, sponsored by this grant, have played a major impact in the award decision. This is a life time achievement of the PI. Other awardees of this Golden Medal are World famous mathematicians, including one Fields Laureate (E.I. Zelmanov).

Protocol Activity Status:

RPPR Final Report
as of 15-Jun-2018

Technology Transfer: A very fruitful collaboration with engineers of US Army Research Laboratory (ARL) Drs. Anders Sullivan and Lam Nguyen is ongoing since 2012. In this collaboration the PI applies his globally convergent numerical methods for Coefficient Inverse Scattering Problems to the experimental data collected by the Forward Looking Radar of ARL. These methods estimate dielectric constants of explosive-like targets It is worth to point out that those experimental data were collected in the field, as opposed to the data collected in a laboratory. The environment was quite cluttered one, which makes our imaging goal much more challenging. Nevertheless, our computational results are quite satisfactory.

The radar community is currently relying only on the energy information of radar images. Unlike this, in our papers with ARL engineers, we compute estimates of dielectric constants of targets. Our hope is that these estimates might help in the future to develop new classification procedures, which would combine the currently used energy information with the estimates of dielectric constants. This combination, in turn might result in lower false alarm rates.

Since 2012 we have published five (5) joint papers in very good journals and one (1) more paper is recently submitted for publication.

In particular, during this reportage period of 06/01/17-05/31/18 we have published the following joint paper with ARL engineers:

M.V. Klibanov, A.E. Kolesov, L. Nguyen and A. Sullivan, Globally strictly convex cost functional for a 1-D inverse medium scattering problem with experimental data, SIAM J. Applied Mathematics, 77 1733-1755, 2017.

And the following joint paper was submitted for publication:

M.V. Klibanov, A.E. Kolesov, A. Sullivan and L. Nguyen, A new version of the convexification method for a 1-D coefficient inverse problem with experimental data, available on www.arxiv.org: 1805.06025, 2018, submitted for publication.

In addition, a ready-to-use software with one of globally convergent numerical methods was transferred to Drs. Anders Sullivan and Lam Nguyen. This software works with those experimental data of ARL.

PARTICIPANTS:

Participant Type: Faculty
Participant: Loc Hoang Nguyen
Person Months Worked: 1.00 **Funding Support:**
Project Contribution:
International Collaboration:
International Travel:
National Academy Member: N
Other Collaborators:

Participant Type: Postdoctoral (scholar, fellow or other postdoctoral position)
Participant: Aleksandr Egor Kolesov
Person Months Worked: 12.00 **Funding Support:**
Project Contribution:
International Collaboration:
International Travel:
National Academy Member: N
Other Collaborators:

Participant Type: Postdoctoral (scholar, fellow or other postdoctoral position)
Participant: Nikolaj Aleksander Koshev
Person Months Worked: 12.00 **Funding Support:**
Project Contribution:
International Collaboration:

International Travel:
National Academy Member: N
Other Collaborators:

Participant Type: PD/PI
Participant: Michael V. Klibanov 6871373
Person Months Worked: 2.00 **Funding Support:**
Project Contribution:
International Collaboration:
International Travel:
National Academy Member: N
Other Collaborators:

Annual Report

US Army Research Laboratory and Office of Army Research grant W911NF-15-1-0233

Grant Title: Globally Convergent Inverse Algorithms via Carleman Weight Functions: Theory, Numerical Studies and Experimental Verifications

Reportage Period: June 1, 2017-May 31, 2018

Principal Investigator: Michael V. Klibanov, Professor, Department of Mathematics and Statistics, University of North Carolina at Charlotte, Charlotte, NC 28223, email: mklibanv@uncc.edu

Abstract

The main topic of this grant is globally convergent numerical methods for Coefficient Inverse Scattering Problems (CISPs). We call a numerical method for a CIP *globally* convergent if a theorem is proved, which claims that this method delivers at least one point in a sufficiently small neighborhood of the exact coefficient without any advanced knowledge of this neighborhood. Currently there are no competitors to the PI on this topic. Target applications of US Army interest are in stand off detection and identification of mine-like targets and improvised explosive devices. In this direction, an active collaboration between the PI and engineers of US Army Research Office Drs. Anders Sullivan and Lam Nguyen is in place see section 4 of this report. We have currently total five (5) joint published papers and one (1) is submitted for publication. Due to an extensive work with experimental microwave data, including the data from the US Army Research Laboratory (ARL), this project is a *truly interdisciplinary* one.

The conventional least squares cost functional for a CISP is non convex. The non-convexity plagues the corresponding optimization method by multiple local minima and ravines, thus, making it necessary to know a good first guess for the solution, which, however, is rarely available in true applications. In fact, the phenomenon of multiple local minima and ravines represents the *major* challenge for numerical methods for CISPs. To handle this challenge, the PI has been working on the development of globally convergent numerical methods for CISPs.

Two types of globally convergent numerical methods (GCMs) for CISPs were developed by the PI: (1) the tail functions method and (2) the convexification method. The convexification GCM is both more promising and more mathematically elegant than the tail functions GCM. In addition, the PI's team has mostly worked on the convexification method during this reportage period and also the tail functions method was described in detail in the previous annual report of the PI. Thus the focus of the current report is on the convexification method.

The convexification constructs a globally strictly convex cost functional J for a CISP. The key element of this functional is the presence of the Carleman Weight Function. This is the function which is involved in the Carleman estimate for the corresponding Partial Differential Operator. The key element of this functional is the presence of the Carleman Weight Function. This is the function which is involved in the Carleman estimate for the corresponding Partial Differential Operator. Furthermore, the convergence of the gradient projection method of the minimization of J to the correct solution of that CISP is guaranteed if starting from any point of a certain bounded domain of an arbitrary diameter. The latter is the *global convergence*.

The PI has been working with the most challenging case of the available data: a single direction of the incident plane wave. This case is the most applicable one in the above problems of Army interest. It has been consistently demonstrated numerically for both computationally simulated and experimental data that globally convergent numerical methods of the PI provide excellent accuracy of the reconstruction of both locations and dielectric constants of targets of interest. In addition, recently the PI has developed a new version

of convexification for the case when either the point source moves along an interval of a straight line or the direction of the incident plane wave changes. It is anticipated, therefore, that this version will provide accurate reconstructions of shapes of targets, on the top of their locations and dielectric constants. The first numerical results on this version for a very popular inverse problem of Electrical Impedance Tomography show promise.

A minor topic of this project is the topic of Phaseless Coefficient Inverse Scattering Problems (PCIPs). In such a problem only the modulus of the complex valued scattered wave field is measured outside of scatterers. Phase is not measured. This topic has applications in imaging of nanostructures and biological cells. Globally convergent methods of the PI are applied in this topic as well as an auxiliary tool. Thus, the main focus of this report is on the topic of the convexification for the case of . And the topic of PCIPs is a minor focus.

TEN MAIN ACHIEVEMENTS OF THIS REPORTAGE PERIOD:

1. The PI got a prestigious award. In August 2017, Sobolev Institute of Mathematics has awarded the PI Golden Medal for "Distinguished Impact in Mathematics". Publications on the topic of Phaseless Inverse Scattering Problems, sponsored by this grant, have played a major impact in the award decision. **This is a life time achievement of the PI.** Other awardees of this Golden Medal are World famous mathematicians, including one Fields Laureate (E.I. Zelmanov).

2. In the case of a single direction of the incident plane wave, the theory of the convexification GCM is developed.

3. Furthermore, the convexification method of item 2 was successfully tested on the *most challenging case: the case of experimental backscattering data for buried mine-like and IED-like targets.* It is demonstrated that the convexification computes very accurately both locations and dielectric constants of these targets. However, shapes are not computed well, see item 4.

4. To accurate compute shapes of targets as well, the PI has recently started to develop an extension of the convexification to the case when either the direction of the incident plane wave is changing or the point source is moving along a straight line. The first computational result shows promise. Nevertheless, many things in this direction still need to be clarified.

5. The classical and very popular inverse problem of Electrical Impedance Tomography (EIT) is solved numerically by the version item 4 of the convexification method. This is the *first* solution of this problem by a *globally convergent numerical method.*

6. The convexification method of item 2 was successfully tested on experimental data collected by engineers of ARL Drs. L. Nguyen and A. Sullivan. During this reportage period one (1) joint paper with Nguyen and Sullivan was published and one (1) was submitted for publication. In the period of 2012-2018 five (5) joint papers were published and one (1) was submitted.

7. Thus, a quite fruitful collaboration of the PI with engineers from ARL has been successfully continued since 2012.

8. Publications during the reportage period acknowledging the support of this grant: nine (9) papers are published and five (5) are submitted for publication. As to the entire period of this funding, June 1, 2015-May 31, 2018, total twenty two (22) papers were published/submitted. All papers are in refereed journals.

9. Two numerical methods for Phaseless Coefficient Inverse Scattering Problem were developed. One of them was successfully tested on experimental data.

10. Publications of the PI with coauthors about Phaseless Coefficient Inverse Scattering Problem constitute the **FIRST SOLUTION** of a long standing problem posed by French mathematicians K. Chadan and P.C. Sabatier in 1977 in their well known book "Inverse Problems in Quantum Scattering Theory", Springer, 1977.

Contents

1 Introduction

The main topic of this grant is globally convergent numerical methods for Coefficient Inverse Scattering Problems (CISPs). Target applications of US Army interest are in the stand off detection and identification of mine-like targets and improvised explosive devices. In this direction, an active collaboration between the PI and engineers of US Army Research Office Drs. Anders Sullivan and Lam Nguyen is in place, see section 4 of this report. We have currently total five (5) joint published papers and one (1) is submitted for publication. Due to an extensive work with backscattering experimental data, including the data from the US Army Research Laboratory (ARL), this project is a *truly interdisciplinary* one.

We call a numerical method for a CIP *globally* convergent if a theorem is proved, which claims that this method delivers at least one point in a sufficiently small neighborhood of the exact coefficient without any advanced knowledge of this neighborhood. Two globally convergent numerical methods (GCMs) were developed by the PI and his coauthors both during the reportage period and during the duration of this funding (2015-2018):

1. The tail functions GCM [2, 4, 5, 8, 15].
2. The convexification GCM [1, 6, 7, 12, 13, 14, 17, 18, 22].

The convexification GCM is both more promising and more mathematically elegant than the tail functions GCM. In addition, the PI's team has mostly worked on the convexification during this reportage period. Thus, the main focus of this annual report is on the convexification GCM. Main achievements are listed in Abstract and are also outlined below.

Below $\mathbf{x} = (x, y, z) \in \mathbb{R}^3$. We assume below that our medium, which occupies the entire space $\mathbb{R}^3$, is isotropic, non-magnetic and is characterized by the spatially distributed dielectric constant $c(\mathbf{x}), \mathbf{x} \in \mathbb{R}^3$, which is also called the relative permittivity. Thus, we model the process of the propagation of the electric field by the Helmholtz equation rather than by the full Maxwell's system. This model was justified numerically in our publications [10, 11]. It was shown in [10, 11] that if the incident electric field has the form $E = (0, E_y, 0)$, then the propagation of the component E_y is well governed by the Helmholtz equation. Another justification comes from the fact that in all our publications on experimental data [2, 4, 5, 8, 12, 24] either Helmholtz equation or its analog for the case of the time domain was used to model the process. Nevertheless, accurate results have been consistently obtained in all these publications.

A minor topic of this project is the topic of Phaseless Coefficient Inverse Scattering Problems (PCIPs). In such a problem only the modulus of the complex valued scattered wave field is measured outside of scatterers. Phase is not measured. This topic has applications in imaging of nanostructures and biological cells. The tail functions globally convergent methods of the PI is applied to this problem as an auxiliary tool. The work on this topic was mostly supported by the ONR grant N00014-15-1-2330 of the PI (2015-2018) and the current ARO funding was used as a leverage. Thus, the topic of PCIPs is a minor focus of this report.

2 Convexification Method in 3-D

We follow in this section our recent publication [12]. In particular, we work here with a of the convexification. This version is more realistic for computations than the continuous versions used some other works of the PI on the convexification. Indeed, "semidiscrete" means that our theory is developed for the case when the differential operator is written in finite differences with respect to two out of three spatial variables, and in the continuous form with respect to the third variable. We impose a computationally reasonable assumption that the grid step size does not tend to zero (unlike the case of some forward problems). The fully discrete case, i.e. when derivatives with all three variables are written in finite differences, is not investigated yet. Indeed, it is well known that this case is a very complicated one.

2.1 Statements of forward and inverse problems

We assume here that we have an incident plane wave propagating along the positive direction of the $z-$axis,

$$u_i(z,k) = e^{ikz}. \tag{2.1}$$

Consider positive numbers $b, d, \xi > 0$. For the convenience for our numerical study, we define now the domain of interest Ω and the backscatter part Γ of its boundary as

$$\Omega = \{\mathbf{x} = (x,y,z) : |x|, |y| < b, z \in (-\xi, d)\}, \tag{2.2}$$

$$\Gamma = \{\mathbf{x} = (x,y,z) : |x|, |y| < b, z = -\xi\}. \tag{2.3}$$

We denote by $c(\mathbf{x})$ the spatially distributed dielectric constant and and let k be the wavenumber. The forward problem for the Helmholtz equation as

$$\Delta u + k^2 c(\mathbf{x}) u = 0, \quad \mathbf{x} \in \mathbb{R}^3, \tag{2.4}$$

$$u(\mathbf{x},k) = u_{\text{sc}}(\mathbf{x},k) + u_i(\mathbf{x},k), \tag{2.5}$$

$$\lim_{r\to\infty} r\left(\partial u_{\text{sc}}/\partial r - iku_{\text{sc}}\right) = 0, \quad r = |\mathbf{x}|. \tag{2.6}$$

Here $u(\mathbf{x},k)$ is the total field, $u_i(\mathbf{x},k)$ is the incident field and $u_{\text{sc}}(\mathbf{x},k)$ is the scattered field satisfying the Sommerfeld radiation condition. This condition means that the scattered field behaves like a outgoing spherical wave far away from the scattering medium.

Also, we assume that the function $c(\mathbf{x})$ satisfies with the following conditions:

$$c(\mathbf{x}) = 1 + \beta(\mathbf{x}), \quad \beta(\mathbf{x}) \geq 0, \mathbf{x} \in \mathbb{R}^3, \quad \text{and } c(\mathbf{x}) = 1, \mathbf{x} \notin \overline{\Omega}. \tag{2.7}$$

The latter equation in assumption (2.7) simply means that the medium outside of Ω is homogeneous (e.g. vacuum). In addition, we assume $c(\mathbf{x}) \in C^{15}(\mathbb{R}^3)$, which is necessary for the validity of the asymptotic behavior of the solution to the direct problem (2.4)–(2.6), see [20, 21]. Note that this kind of smoothness condition is typically not of a significant concern for CIPs, see, e.g. Theorem 4.1 in [42]. From Lemma 3.3 of [2] we also know that

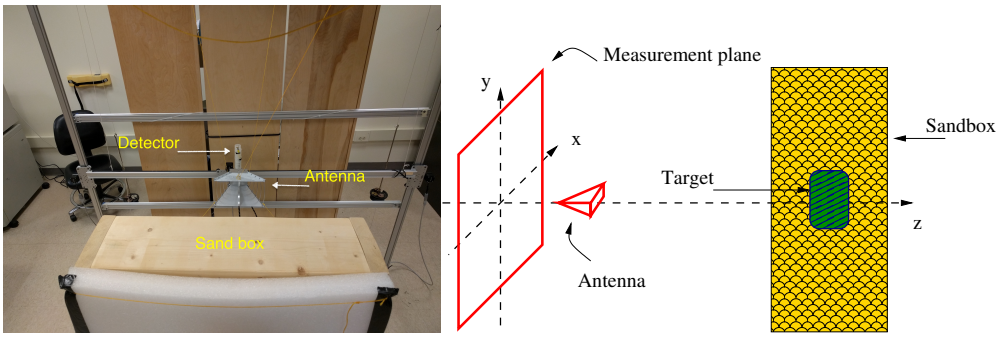

Figure 1: *a) The photograph of our experimental device. Mine-like targets are buried in this sandbox. b) Schematic diagram of our measurements of backscattering data.*

the derivative $\partial_k u(\mathbf{x}, k)$ exists for all $\mathbf{x} \in \mathbb{R}^3, k > 0$ and holds the same smoothness condition as $u(\mathbf{x}, k)$.

Let $\Gamma \subset \partial\Omega$ be the "backscattering" part of $\partial\Omega$ (see Figure 1 for an illustration). We are interested in the following coefficient inverse scattering problem:

Coefficient Inverse Scattering Problem (CISP). *Let Ω and $\Gamma \subset \partial\Omega$ be as in (2.2) and (2.3). Let $[\underline{k}, \overline{k}] \subset (0, \infty)$ be the interval of wavenumbers. Assume that we are given the boundary data $g_0(\mathbf{x}, k)$ as*

$$u(\mathbf{x}, k) = g_0(\mathbf{x}, k), \quad \mathbf{x} \in \Gamma,\ k \in [\underline{k}, \overline{k}]. \tag{2.8}$$

Determine the function $c(\mathbf{x})$ for $\mathbf{x} \in \Omega$.

Actually the function u is measured far from the domain of interest Ω. Next, using the data propagation procedure, one can compute functions g_0 and g_1, where

$$u_z(\mathbf{x}, k) = g_1(\mathbf{x}, k), \quad \mathbf{x} \in \Gamma,\ k \in [\underline{k}, \overline{k}]. \tag{2.9}$$

Even though we use the data propagation in our computations below, we do not describe it here for brevity. Instead, we refer to [4, 8] for detailed discussions of this procedure, including the previous report on this grant [23]. In fact, this procedure is widely used in optics with the name *angular spectrum representation*.

We additionally complement Dirichlet (2.8) and Neumann (2.9) boundary data on Γ as

$$u(\mathbf{x}, k) = e^{ikz}, \quad \mathbf{x} \in \partial\Omega \setminus \Gamma, k \in [\underline{k}, \overline{k}]. \tag{2.10}$$

Condition (2.10) simply means that we extend the scattered field by zero on the rest of the boundary of Ω. It was demonstrated in [2, 4, 12] that this data extension works quite well for both cases of simulated and experimental data.

We now briefly describe the travel time $\tau(\mathbf{x})$ which is important in our analysis. The Riemannian metric generated by $c(\mathbf{x})$ is:

$$d\tau(\mathbf{x}) = \sqrt{c(\mathbf{x})}|d\mathbf{x}|, \quad |d\mathbf{x}| = \sqrt{(dx)^2 + (dy)^2 + (dz)^2}.$$

Let us fix a number $a > \max(\xi, 0)$. And consider the plane P_a,

$$P_a = \{(x, y, -a) : x, y \in \mathbb{R}\}. \tag{2.11}$$

Since $a > \xi$, then by (2.2) $\Omega \subset \{z > -a\}$. We impose from now on the following assumption on $c(\mathbf{x})$.

Regularity Assumption. *For any point $\mathbf{x} \in \mathbb{R}^3$ there exists a unique geodesic line $\Gamma(\mathbf{x}, a)$, with respect to metric $d\tau$, connecting $\mathbf{x}$ with the plane P_a and perpendicular to P_a at the intersection point.*

A sufficient condition of the regularity of geodesic lines is [43]:

$$\sum_{i,j=1}^{3} \frac{\partial^2 \ln(c(\mathbf{x}))}{\partial x_i \partial x_j} \xi_i \xi_j \geq 0, \quad \text{for all } \mathbf{x} \in \overline{\Omega}, \boldsymbol{\xi} \in \mathbb{R}^3.$$

As in [21] we define the travel time $\tau(\mathbf{x})$ from the plane P_a to the point $\mathbf{x}$:

$$\tau(\mathbf{x}) = \int\limits_{\Gamma(\mathbf{x},a)} \sqrt{c(\boldsymbol{\xi})} d\sigma.$$

2.2 The Integro-Differential Equation

In this section we reformulate our coefficient inverse problems as an integro-differential equation.

2.2.1 Asymptotics

First, we use the high frequency asymptotic behavior of the function $u(\mathbf{x}, k)$. It was shown in [50] (theorem 17) and later modified in [21] that

$$u(\mathbf{x}, k) = A(\mathbf{x}) e^{ik(\tau(\mathbf{x}) - a)} \left[1 + s(\mathbf{x}, k)\right], \quad \mathbf{x} \in \overline{\Omega}, k \to \infty, \tag{2.12}$$

where $\tau(\mathbf{x})$ is the travel time introduced in the previous section, $A(\mathbf{x}) > 0$ and $s(\mathbf{x}, k)$ satisfies

$$s(\mathbf{x},k) = O\left(\frac{1}{k}\right), \quad \partial_k s(\mathbf{x},k) = O\left(\frac{1}{k}\right), \quad \mathbf{x} \in \overline{\Omega}, k \to \infty. \tag{2.13}$$

Now we define

$$w(\mathbf{x}, k) = \frac{u(\mathbf{x}, k)}{u_i(\mathbf{x}, k)}. \tag{2.14}$$

It follows from (4.24), (2.12) and (2.14) that

$$w(\mathbf{x}, k) = A(\mathbf{x}) e^{ik(\tau(\mathbf{x}) - z - a)} [1 + s(\mathbf{x}, k)], \quad \mathbf{x} \in \overline{\Omega}, k \to \infty. \tag{2.15}$$

Using (2.15) we define $\log w(\mathbf{x},k)$ for large values of $\underline{k}$ as:

$$\log w(\mathbf{x},k) = \ln A(\mathbf{x}) + ik(\tau(\mathbf{x}) - z - a) + \sum_{n=1}^{\infty} \frac{(-1)^{n-1}}{n} \left(s(\mathbf{x},k)\right)^n. \tag{2.16}$$

It is obvious from (2.16) that

$$\exp\left[\ln A(\mathbf{x}) + ik(\tau(\mathbf{x}) - z - a) + \sum_{n=1}^{\infty} \frac{(-1)^{n-1}}{n} \left(s(\mathbf{x},k)\right)^n\right]$$

$$= A(\mathbf{x}) e^{ik(\tau(\mathbf{x})-z-a)}[1 + s(\mathbf{x},k)].$$

Hence, the right hand side of (2.16) uniquely defines $\log w(\mathbf{x},k)$.

2.2.2 Integro-differential equation

For $\mathbf{x} \in \Omega$, $k \in [\underline{k}, \overline{k}]$ consider the function $v(\mathbf{x},k)$,

$$v(\mathbf{x},k) = \frac{\log w(\mathbf{x},k)}{k^2}. \tag{2.17}$$

Then

$$\Delta v + k^2 \nabla v \cdot \nabla v = -c(\mathbf{x}). \tag{2.18}$$

Define the function $q(\mathbf{x},k)$ as

$$q(\mathbf{x},k) = \partial_k v(\mathbf{x},k). \tag{2.19}$$

Hence,

$$v(\mathbf{x},k) = -\int_k^{\overline{k}} q(\mathbf{x},\kappa) d\kappa + V(\mathbf{x}), \tag{2.20}$$

where $V(\mathbf{x})$ is the so-called tail function,

$$V(\mathbf{x}) = v(\mathbf{x},\overline{k}). \tag{2.21}$$

It follows from (4.24), (2.7) and (2.14) that

$$\Delta w + k^2 \beta w + 2ikw_z = 0. \tag{2.22}$$

Using (2.17), we obtain from (2.22)

$$\Delta v + k^2 \nabla v \cdot \nabla v + 2ikv_z + \beta(\mathbf{x}) = 0.$$

To eliminate $\beta(\mathbf{x})$ we differentiate this equation with respect to k,

$$\Delta q + 2k\nabla v \cdot (k\nabla q + \nabla v) + 2i\left(k\frac{\partial q}{\partial z} + \frac{\partial v}{\partial z}\right) = 0. \tag{2.23}$$

Substituting (2.20) in (2.23) we obtain our target integro-differential equation

$$L(q) = \Delta q + 2k\left(\nabla V - \int_k^{\overline{k}} \nabla q(s)ds\right)\cdot\left(k\nabla q + \nabla V - \int_k^{\overline{k}} \nabla q\,(s)\,ds\right) \\ +2i\left(kq_z + V_z - \int_k^{\overline{k}} q_z\,(\kappa)\,ds\right) = 0. \tag{2.24}$$

We complement equation (2.24) with the overdetermined boundary conditions:

$$q(\mathbf{x},k) = \phi_0(\mathbf{x},k), \quad q_z(\mathbf{x},k) = \phi_1(\mathbf{x},k), \quad \mathbf{x}\in\Gamma,\ k\in[\underline{k},\overline{k}], \\ q(\mathbf{x},k) = 0, \quad \mathbf{x}\in\partial\Omega\setminus\Gamma,\ k\in[\underline{k},\overline{k}], \tag{2.25}$$

where the functions ϕ_0 and ϕ_1 are computed from the functions g_0 and g_1 in (2.8), (2.9). The third boundary condition (2.25) easily follows from (2.10), (2.14), (2.17) and (2.19).

We have two unknown functions in (2.24): $q(\mathbf{x},k)$ and $V(\mathbf{x})$. Hence, we solve the problem (2.24), (2.25) using a predictor-corrector method. First, we find an approximation of $V(\mathbf{x})$ use it as a predictor. Next, we approximate the function $q(\mathbf{x},k)$. As soon as certain approximations of $q(\mathbf{x},k)$ and $V(\mathbf{x})$ are found, an approximation for the target coefficient $c(\mathbf{x})$ can be computed via (2.18) and (2.20) for some $k\in[\underline{k},\overline{k}]$. In our computations we use $k=\overline{k}$. We hence focus below on the approximations of functions $q(\mathbf{x},k)$ and $V(\mathbf{x})$.

2.3 Approximation of the tail function

In this section we present a method for finding an approximation of the tail function $V(\mathbf{x})$.

It follows from (2.12) and (2.17) that there exists a function $p(\mathbf{x})$ such that

$$v(\mathbf{x},k) = \frac{p(\mathbf{x})}{k} + O\left(\frac{1}{k^2}\right), \quad q(\mathbf{x},k) = -\frac{p(\mathbf{x})}{k^2} + O\left(\frac{1}{k^3}\right), \quad k\to\infty,\ \mathbf{x}\in\Omega.$$

For sufficiently large $\overline{k}$, we drop $O(1/\overline{k}^2)$ and $O(1/\overline{k}^3)$ and set

$$V(\mathbf{x}) = v(\mathbf{x},\overline{k}) = \frac{p(\mathbf{x})}{\overline{k}}, \quad q(\mathbf{x},\overline{k}) = -\frac{p(\mathbf{x})}{\overline{k}^2}, \mathbf{x}\in\Omega. \tag{2.26}$$

Next, substituting (2.26) in (2.16) and setting $k=\overline{k}$, we obtain

$$\Delta V(\mathbf{x}) = 0, \quad \mathbf{x}\in\Omega. \tag{2.27}$$

This equation is supplemented by the following boundary conditions:

$$V(\mathbf{x}) = \psi_0(\mathbf{x}), \quad V_z(\mathbf{x}) = \psi_1(\mathbf{x}), \quad \mathbf{x}\in\Gamma, \quad V(\mathbf{x}) = 0, \quad \mathbf{x}\in\partial\Omega\setminus\Gamma, \tag{2.28}$$

where functions ψ_0 and ψ_1 are computed using (2.25) and (2.26). Due to the approximation in (2.27), we have observed that if we drop the second boundary condition $V_z(\mathbf{x})\mid_\Gamma = \psi_1(\mathbf{x})$ in (2.28) and find $V(\mathbf{x})$ by solving the resulting Dirichlet boundary value problem for Laplace equation (2.27) with the boundary data (2.28), the result is not satisfactory.

2.4 Partial Finite Differences

Following our above idea (beginning of section 2) to work with a semidiscrete version of our method, we present this version in this section 2.3.

2.4.1 Grid points

We now write differential operators in (2.24) and (2.27) in finite differences with respect to x, y. Let the domain $\Omega_1 \subset \mathbb{R}^2$ be the orthogonal projection of the domain $\Omega \subset \mathbb{R}^3$ in (2.2) on the plane $\{z = 0\}$,

$$\Omega_1 = \{(x, y, z) : |x| < b, |y| < b, z = 0\}.$$

Consider a finite difference grid in Ω_1 with the uniform grid step size h. This grid consists of points $\{(x_j, y_s)\}_{j,s=1}^{N_h} \subset \overline{\Omega}_1$. Denote

$$\Omega_h = \{(x_j, y_s, z) : (x_j, y_s)_{j,s=1}^{N_h} \subset \overline{\Omega}_1, z \in (-\xi, d)\}. \tag{2.29}$$

For every interior point $(x_j, y_s, z) \in \overline{\Omega} \setminus \partial\Omega$ four neighboring points are:

$$\begin{aligned} (x_{j+1}, y_s, z) &= (x_j + h, y_s, z), \quad (x_{j-1}, y_s, z) = (x_j - h, y_s, z), \\ (x_j, y_{s+1}, z) &= (x_j, y_s + h, z), \quad (x_j, y_{s-1}, z) = (x_j, y_s - h, z). \end{aligned}$$

The corresponding Laplace operator written in partial finite differences is

$$\Delta^h u = u_{zz} + u^h_{xx} + u^h_{yy}, \tag{2.30}$$

where u^h_{xx} and u^h_{yy} are finite difference analogs of continuous derivatives u_{xx} and u_{yy},

$$u^h_{xx}(x_j, y_s, z) = \frac{u(x_j - h, y_s, z) - 2u(x_j, y_s, z) + u(x_j + h, y_s, z)}{h^2} \tag{2.31}$$

and similarly for u^h_{yy}. Next,

$$\nabla^h u = (\partial^h_x u, \partial^h_y u, \partial_z u), \tag{2.32}$$

where

$$\partial^h_x u(x_j, y_s, z) = \frac{u(x_j + h, y_s, z) - u(x_j - h, y_s, z)}{2h}$$

and similarly for $\partial^h_y u(x_j, y_s, z)$.

2.5 Problems (2.24)–(2.25) and (2.27)–(2.28) in partial finite differences

We now rewrite problem (2.24)–(2.25) in partial finite differences. To this end, we keep in mind that only interior grid points are involved in differential operators below. Using

(2.29)–(2.32), we obtain for $x \in \Omega_h$

$$L^h(q) = \Delta^h q + 2k\left(\nabla^h V - \int_k^{\overline{k}} \nabla^h q(\kappa) d\kappa\right) \cdot \left(k\nabla^h(q+V) - \int_k^{\overline{k}} \nabla^h q\,(\kappa)\, d\kappa\right) + 2i\left(kq_z + V_z - \int_k^{\overline{k}} q_z\,(\kappa)\, d\kappa\right) = 0, \tag{2.33}$$

$$q(\mathbf{x},k) = \phi_0(\mathbf{x},k), \quad q_z(\mathbf{x},k) = \phi_1(\mathbf{x},k), \quad \mathbf{x} \in \Gamma,\ k \in [\underline{k},\overline{k}], \qquad q(\mathbf{x},k) = 0, \quad \mathbf{x} \in \partial\Omega \setminus \Gamma,\ k \in [\underline{k},\overline{k}]. \tag{2.34}$$

Similarly, problem (2.24)–(2.25) becomes

$$\Delta^h V(\mathbf{x}) = 0, \quad \mathbf{x} \in \Omega. \tag{2.35}$$

$$V(\mathbf{x}) = \psi_0(\mathbf{x}), \quad V_z(\mathbf{x}) = \psi_1(\mathbf{x}), \quad \mathbf{x} \in \Gamma, \quad V(\mathbf{x}) = 0, \quad \mathbf{x} \in \partial\Omega \setminus \Gamma. \tag{2.36}$$

Remarks 2.1:

1. Below in this section, functions $q(\mathbf{x},k)$ and $V(\mathbf{x})$, and other functions we consider are semidiscrete, i.e. they are defined on $\overline{\Omega}_h$. This means that, e.g. $q(\mathbf{x},k) = \{q(x_j,y_s,z)\}_{j,s=1}^{N_h}$, $V(\mathbf{x}) = \{V(x_j,y_s,z)\}_{j,s=1}^{N_h}$, etc. Boundary conditions at $\partial\Omega$ for the functions q and V are also defined only on grid points which belong to the boundary $\partial\Omega$.

2. Since the grid step size h is not changing in our arrangement, we will not indicate below for brevity the dependence of some parameters on h, although they do depend on h. Thus, for example below $C = C(\xi,d) > 0$ denotes different positive constants that depend only on numbers ξ,d and h.

2.6 Some functional spaces

Denote by $\overline{z}$ the complex conjugate of $z \in \mathbb{C}$. For the convenience of the presentation, we consider any complex valued function $U = \operatorname{Re} U + i \operatorname{Im} U = U_1 + iU_2$ as the 2D vector function $U = (U_1, U_2)$. Furthermore, each component U_j of this vector function is, in turn, another vector function defined on the above grid, $U_j = U_j(x_j, y_s, z, k)$. Hence, below any Banach space of complex valued functions is actually the space of these real valued vector functions with the well known definitions of norms and scalar products (if in Hilbert spaces). For brevity we do not distinguish below complex valued functions and corresponding vector functions.

We introduce the Hilbert spaces $H^{2,h}(\Omega_h)$, $L_2^h(\Omega_h)$ and H_n^h of semidiscrete complex valued

functions as

$$H^{2,h}(\Omega_h) = \{f(x_j, y_s, z) : \|f\|^2_{H^{n,h}(\Omega_h)} = \sum_{j,s=1}^{N_h} \sum_{r=0}^{2} h^2 \int\limits_{-\xi}^{d} \left|\partial_z^r f\left(x_j, y_s, z\right)\right|^2 dz < \infty\},$$

$$L_2^h\left(\Omega_h\right) = \{f(x_j, y_s, z) : \|f\|^2_{L_2^h(\Omega_h)} = \sum_{j,s=1}^{N_h} h^2 \int\limits_{-\xi}^{d} \left|f\left(x_j, y_s, z\right)\right|^2 dz < \infty\},$$

$$H_n^h = \{f(x_j, y_s, z, k) : \|f\|^2_{H_n^h} = \int\limits_{\underline{k}}^{\overline{k}} \left\|f\left(\mathbf{x}, k\right)\right\|^2_{H^{n,h}(\Omega_h)} dk < \infty\}, \quad n = 2, 3.$$

Denote by $[\,,]$ the scalar product in $H^{2,h}(\Omega_h)$. We also define subspaces $H_0^{2,h}(\Omega_h) \subset H^{2,h}(\Omega_h)$ and $H_{0,2}^h \subset H_2^h$ as

$$H_0^{2,h}(\Omega_h) = \{f(x_j, y_s, z) \in H^{2,h}(\Omega_h) : f(\mathbf{x}) \mid_{\partial\Omega} = 0, \partial_n f(\mathbf{x}) \mid_{\Gamma} = 0\},$$
$$H_{0,2}^h = \{f(x_j, y_s, z, k) \in H_2^h : f(\mathbf{x}, k) \mid_{\partial\Omega} = 0, f_z(\mathbf{x}, k) \mid_{\Gamma} = 0, \forall k \in [\underline{k}, \overline{k}]\}.$$

Note that since, for all $f \in H_{0,2}^h$,

$$f(x_j, y_s, z, k) = \int\limits_{-\xi}^{z} f_z(x_j, y_s, \rho, k) d\rho, \quad f_z(x_j, y_s, z, k) = \int\limits_{-\xi}^{z} f_{zz}(x_j, y_s, \rho, k) d\rho,$$

then the norm in $H_{0,2}^h$ is equivalent with

$$\|f(\mathbf{x})\|^2_{H_{0,2}^h(\Omega_h)} = \sum_{j,s=1}^{N_h} h^2 \int\limits_{-\xi}^{d} \left|\Delta^h f(x_j, y_s, z)\right|^2 dz. \tag{2.37}$$

In addition, for $l = 0, 1$

$$C^l(\overline{\Omega}_h) = \{f(x_j, y_s, z) : \|f\|_{C^l(\overline{\Omega}_h)} = \max_{j,s} \|f(x_j, y_s, z)\|_{C^l[-\xi,d]} < \infty\},$$
$$C_l^h = \{f(x_j, y_s, z, k) : \|f\|_{C_l^h} = \max_{k \in [\underline{k}, \overline{k}]} \|f(x_j, y_s, z, k)\|_{C^l(\overline{\Omega}_h)} < \infty\}.$$

By embedding theorem $H^{2,h}(\Omega_h) \subset C^1(\overline{\Omega}_h), H_n^h \subset C_{n-1}^h$ and

$$\|f\|_{C^1(\overline{\Omega}_h)} \leq C \|f\|_{H^{2,h}(\Omega_h)}, \quad \text{for all } f \in H^{2,h}(\Omega_h), \tag{2.38}$$
$$\|f\|_{C_{n-1}^h} \leq C \|f\|_{H_n^h}, \quad \text{for all } f \in H_n^h. \tag{2.39}$$

2.7 Two Cost Functionals with CWFs

Thus, the CWF we use to solve problems (2.33)–(2.34) and (2.35)–(2.36) is:

$$\varphi_\lambda(z) = e^{-2\lambda z}. \tag{2.40}$$

2.7.1 Problem (2.35)–(2.36)

First, we present the cost functional for the solution of problem (2.35)–(2.36) which is about the tail function. Non-zero boundary conditions in (2.36) are inconvenient for us. Hence, we assume that there exists a function $Q(\mathbf{x}) \in H^{2,h}(\Omega_h)$ such that

$$Q(\mathbf{x}) = \psi_0(\mathbf{x}), \quad \partial_z Q(\mathbf{x}) = \psi_1(\mathbf{x}), \quad \mathbf{x} \in \Gamma; \quad Q(\mathbf{x}) = 0, \quad \mathbf{x} \in \partial\Omega \setminus \Gamma, \tag{2.41}$$

Define

$$W(\mathbf{x}) = V(\mathbf{x}) - Q(\mathbf{x}) \in H_0^{2,h}(\Omega_h). \tag{2.42}$$

Hence, we consider the following minimization problem:

Minimization Problem 1. *For $W \in H_0^{2,h}(\Omega_h)$, minimize the functional $I_\mu(W)$,*

$$I_\mu(W) = e^{2\mu d} \sum_{j,s=1}^{N_h} h^2 \int_{-\xi}^{d} \left|(\Delta^h W + \Delta^h Q)(x_j, y_s, z)\right|^2 \varphi_\mu(z) dz. \tag{2.43}$$

The multiplier $e^{2\mu d}$ is introduced here to ensure that $e^{2\mu d} \min_{[-\xi,d]} \varphi_\mu(z) = 1$.

Now following the Tikhonov regularization concept [48], we assume that there exists an exact solution $V_*(\mathbf{x})$ of the problem (2.35)–(2.36) with the noiseless data $\psi_{0*}(\mathbf{x})$ and $\psi_{1*}(\mathbf{x})$. Below the subscript "$*$" is related only to the exact solution. In fact the data $\psi_0(\mathbf{x})$ and $\psi_1(\mathbf{x})$ contain noise, we therefore denote by $\delta \in (0,1)$ the level of noise in the data $\psi_0(\mathbf{x})$ and $\psi_1(\mathbf{x})$. Again, following the same concept, we should assume that δ is sufficiently small. Suppose that there exists function $Q_*(\mathbf{x}) \in H^{2,h}(\Omega_h)$ such that

$$Q_*(\mathbf{x}) = \psi_{0*}(\mathbf{x}), \quad \partial_z Q_*(\mathbf{x}) = \psi_{1*}(\mathbf{x}), \quad \mathbf{x} \in \Gamma; \quad Q_*(\mathbf{x}) = 0, \quad \mathbf{x} \in \partial\Omega \setminus \Gamma, \tag{2.44}$$

$$\|Q - Q_*\|_{H^{2,h}(\Omega_h)} < \delta, \tag{2.45}$$

where Q is defined in (2.41). We will choose in Theorem 2.2 a certain dependence $\mu = \mu(\delta)$ of the parameters μ on the noise level δ. Denote $W_{\mu(\delta)}(\mathbf{x}) = W_{\min}(\mathbf{x})$ the unique minimizer of the functional $I_{\mu(\delta)}(W)$ (Theorem 2.2) and by (2.42) let

$$V_{\mu(\delta)}(\mathbf{x}) = W_{\mu(\delta)}(\mathbf{x}) + Q(\mathbf{x}) = W_{\min}(\mathbf{x}) + Q(\mathbf{x}). \tag{2.46}$$

2.7.2 Problem (2.33)–(2.34)

Assume that there exists function $F(\mathbf{x}, k) \in H_3^h$ such that (see (6.10)):

$$F(\mathbf{x}, k) = \phi_0(\mathbf{x}, k),\ F_z(\mathbf{x}, k) = \phi_1(\mathbf{x}, k), \quad \mathbf{x} \in \Gamma, \quad F(\mathbf{x}, k) = 0, \quad \mathbf{x} \in \partial\Omega \setminus \Gamma, \tag{2.47}$$

and that there exists exact solution $c_*(\mathbf{x})$ to the CIP satisfying the conditions for $c(\mathbf{x})$ and generating noiseless data $\phi_{0,*}$ and $\phi_{1,*}$ in (2.44). We also assume that there exists the function $F_*(\mathbf{x}, k) \in H_3^h$ satisfying the following analog of boundary conditions (2.47):

$$F_*(\mathbf{x}, k) = \phi_{0,*}(\mathbf{x}, k),\ \partial_z F_*(\mathbf{x}, k) = \phi_{1,*}(\mathbf{x}, k),\ \mathbf{x} \in \Gamma,\ F_*(\mathbf{x}, k) = 0,\ \mathbf{x} \in \partial\Omega \setminus \Gamma. \tag{2.48}$$

We assume that

$$\|F - F_*\|_{H_3^h} < \delta. \tag{2.49}$$

Let $q_* \in H_2^h$ be the function q generated by $c_*(\mathbf{x})$. We define p and p_* as

$$p(\mathbf{x}, k) = q(\mathbf{x}, k) - F(\mathbf{x}, k), \quad p_*(\mathbf{x}, k) = q_*(\mathbf{x}, k) - F_*(\mathbf{x}, k). \tag{2.50}$$

Therefore, the functions p and $p_* \in H_{0,2}^h$. Now consider an arbitrary number $R > 0$ and a ball $B(R) \subset H_{0,2}^h$ of the radius R,

$$B(R) = \{r \in H_{0,2}^h : \|r\|_{H_2^h} < R\}. \tag{2.51}$$

Using the integro-differential equation (6.8), boundary conditions (6.10) for it, (2.47), (2.48) and (2.50), we construct our cost functional $J_\lambda(p)$ with the CWF (2.40) in it as:

$$J_\lambda(p) = e^{2\lambda d} \sum_{j,s=1}^{N_h} h^2 \int\limits_{\underline{k}}^{\overline{k}} \int\limits_{-\xi}^{d} |L^h(p+F)(x_j, y_s, z, \kappa)|^2 \varphi_\lambda(z) dz d\kappa, \quad p \in \overline{B(R)}, \tag{2.52}$$

where the tail function in L^h is defined in (2.46). Similarly with (2.43), the multiplier $e^{2\lambda d}$ is introduced to balance two terms in the right hand side of (2.52). We have the following optimization problem:

Minimization Problem 2. *Minimize the functional $J_\lambda(p)$ on the set $p \in \overline{B(R)}$.*

2.8 Carleman estimate and global strict convexity

In this section we study the minimization problems 1 and 2 of sections 2.6.1 and 2.6.2. First, we are concerned with the Carleman estimate with the CWF (2.40).

Theorem 2.1 (Carleman estimate). *For $\lambda > 0$ let*

$$B_h(u, \lambda) = \sum_{j,s=1}^{M_h} h^2 \int\limits_{-\xi}^{d} |\Delta^h u(x_j, y_s, z)|^2 \varphi_\lambda(z) dz.$$

Then there exists a sufficiently large number $\lambda_0 = \lambda_0(\xi, d) > 1$ such that for all $\lambda \geq \lambda_0$ the following estimate is valid for all functions $u \in H_0^{2,h}(\Omega_h)$

$$B_h(u, \lambda) \geq C \sum_{j,s=1}^{M_h} h^2 \int\limits_{-\xi}^{d} |u_{zz}(x_j, y_s, z)|^2 \varphi_\lambda(z) dz + C\lambda \sum_{j,s=1}^{M_h} h^2 \int\limits_{-\xi}^{d} |u_z(x_j, y_s, z)|^2 \varphi_\lambda(z) dz$$
$$+ C\lambda^3 \sum_{j,s=1}^{M_h} h^2 \int\limits_{-\xi}^{d} |u(x_j, y_s, z)|^2 \varphi_\lambda(z) dz. \tag{2.53}$$

The next theorem is about the functional $I_\mu(W)$ in (2.43).

Theorem 2.2. *Let $W \in H_0^{2,h}(\Omega_h)$ be the function in (2.42). Suppose that there exists $Q \in H^{2,h}(\Omega_h)$ satisfying conditions (2.44). Then for each $\mu > 0$ there exists unique minimizer $W_\mu \in H_0^{2,h}(\Omega_h)$ of the functional (2.43). Suppose now that there exists an exact solution $V_* \in H^{2,h}(\Omega_h)$ of equation (2.27) with the boundary data $\psi_{0*}(x)$ and $\psi_{1*}(x)$ in (2.28). Also, assume that there exists a function $Q_* \in H^{2,h}(\Omega_h)$ satisfying conditions (2.44) and such that inequality (2.45) holds, where $\delta \in (0,1)$ is the noise level in the data. Let $\lambda_0 > 0$ be the number in Theorem 2.1. Choose $\delta_0 \in (0, e^{-2(d+\xi)\lambda_0})$. For any $\delta \in (0, \delta_0)$ let*

$$\mu = \mu(\delta) = \ln(\delta^{-1/(2(d+\xi))}). \tag{2.54}$$

Let the function $V_{\mu(\delta)}(\mathbf{x})$ be defined via (2.46). Then the following convergence estimate of $V_{\mu(\delta)}(\mathbf{x})$ to the exact solution $V_*(\mathbf{x})$ holds as $\delta \to 0$

$$\left\| V_{\mu(\delta)} - V_* \right\|_{H^{2,h}(\Omega_h)} \leq C\sqrt{\delta}. \tag{2.55}$$

In addition, $V_{\mu(\delta)} \in C^1(\overline{\Omega}_h)$ and

$$C \left\| \nabla V_{\mu(\delta)} \right\|_{C^1(\overline{\Omega}_h)} \leq \left\| V_{\mu(\delta)} \right\|_{H^{2,h}(\Omega_h)} \leq C \left[1 + \| V_* \|_{H^{2,h}(\Omega_h)} \right]. \tag{2.56}$$

The main analytical result of this section is Theorem 2.3.

Theorem 2.3 (globally strict convexity). *Assume that conditions of Theorem 2.2 hold. Let $\lambda_1 \geq \lambda_0$ be the number defined below in the formulation of this theorem. Assume that there exist functions $F(\mathbf{x}, k)$, $F_*(\mathbf{x}, k) \in H_3^h$ satisfying conditions (2.47)–(2.49), where $\delta \in (0, \delta_1)$ and $\delta_1 \in (0, e^{-2(d+\xi)\lambda_1})$. Set in (2.52) $V = V_{\mu(\delta)}$, where the function $V_{\mu(\delta)}$ is defined in Theorem 2.2. First, the functional $J_\lambda(p)$ has the Frechét derivative $J'_\lambda(p) \in H_{0,2}^h$ at any point $p \in H_{0,2}^h$. Second, there exist numbers*

$$\lambda_1 = \lambda_1(\Omega_h, R, \|F_*\|_{H_3^h}, \|V_*\|_{H^{2,h}(\Omega_h)}, \underline{k}, \overline{k}) \geq \lambda_0,$$
$$C_1 = C_1(\Omega_h, R, \|F_*\|_{H_3^h}, \|V_*\|_{H^{2,h}(\Omega_h)}, \underline{k}, \overline{k}) > 0,$$

that depend only on the listed parameters, such that for any $\lambda \geq \lambda_1$ the functional $J_\lambda(p)$ is strictly convex on $\overline{B(R)}$. In other words, the following estimate holds:

$$J_\lambda(p+r) - J_\lambda(p) - J'_\lambda(p)(r) \geq C_1 \|r\|^2_{H_2^h}, \quad \text{for all } p, p+r \in \overline{B(R)}. \tag{2.57}$$

Denote $P_{\overline{B}} : H_{0,2}^h \to \overline{B(R)}$ the projection of the Hilbert space $H_{0,2}^h$ on $\overline{B(R)} \subset H_{0,2}^h$. Let p_0 be an arbitrary point in $B(R)$ and $\gamma \in (0,1)$. Consider the following sequence:

$$p_n = P_{\overline{B}}(p_{n-1} - \gamma J'_\lambda(p_{n-1})), \ n = 1, 2, \ldots \tag{2.58}$$

The following theorem follows from the combination of Theorem 2.3 with Lemma 2.1 and Theorem 2.1 of [17].

Theorem 2.4. *Suppose that conditions of Theorems 2.2 and 2.3 are satisfied. Let* $\lambda \geq \lambda_1$, *where* λ_1 *is defined in Theorem 2.3. Then there exists unique minimizer* $p_{\min,\lambda} \in \overline{B(R)}$ *of the functional* $J_\lambda(p)$ *on the set* $\overline{B(R)}$ *and*

$$J'_\lambda(p_{\min,\lambda})(y - p_{\min,\lambda}) \geq 0, \quad \text{for all } y \in H^h_{0,2}. \tag{2.59}$$

Also, there exists a sufficiently small number $\gamma_0 = \gamma_0(\Omega_h, R, \|F_*\|_{H^h_3}, \|V_*\|_{H^{2,h}(\Omega_h)}, \underline{k}, \overline{k}, \lambda) \in (0,1)$ *that depends only on the listed parameters such that for any* $\gamma \in (0, \gamma_0)$ *the sequence (4.42) converges* $p_{\min,\lambda}$,

$$\|p_{\min,\lambda} - p_n\|_{H^h_2} \leq \theta^n \|p_{\min,\lambda} - p_0\|_{H^h_2}, \quad n = 1, 2, \ldots \tag{2.60}$$

where the number $\theta = \theta(\Omega_h, R, \|F_*\|_{H^h_3}, \|V_*\|_{H^{2,h}(\Omega_h)}, \underline{k}, \overline{k}, \lambda, \gamma) \in (0,1)$ *depends only on listed parameters.*

Thus, (2.60) estimates the convergence rate of the sequence (4.42) to the minimizer $p_{\min,\lambda}$. We now need to estimate the convergence rate of this sequence to the exact solution. To do this, we follow the Tikhonov regularization concept [48] in Theorem 2.5 via assuming that the exact solution $p_* \in B(R)$.

Theorem 2.5 (accuracy estimate and global convergence of the gradient projection method). *Assume that conditions of Theorems 2.2 and 2.3 are satisfied. Let* λ_1 *be the number of Theorem 2.3,* $\delta_1 \in (0, e^{-4(d+\xi)\lambda_1})$ and $\delta \in (0, \delta_1)$. *Set* $\lambda = \lambda(\delta) = \ln(\delta^{-1/(4(d+\xi))}) > \lambda_1$. *Furthermore, assume that the function* $p_* \in B(R)$. *Then there exists a number*

$$C_2 = C_2(\Omega_h, R, \|F_*\|_{H^h_3}, \|V_*\|_{H^{2,h}(\Omega_h)}, \underline{k}, \overline{k}) > 0$$

depending only on the listed parameters such that

$$\left\|p_* - p_{\min,\lambda(\delta)}\right\|_{H^h_2} \leq C_2 \delta^{1/4}, \tag{2.61}$$

$$\left\|c_* - c_{\min,\lambda(\delta)}\right\|_{L^h_2(\Omega_h)} \leq C_2 \delta^{1/4}. \tag{2.62}$$

In addition, we have the following convergence estimates

$$\|p_* - p_n\|_{H^h_2} \leq C_2 \delta^{1/4} + \theta^n \left\|p_{\min,\lambda(\delta)} - p_0\right\|_{H^h_2}, \ n = 1, 2, \ldots \tag{2.63}$$

$$\|c_* - c_n\|_{L^h_2(\Omega_h)} \leq C_2 \delta^{1/4} + \theta^n \left\|p_{\min,\lambda(\delta)} - p_0\right\|_{H^h_2}, \ n = 1, 2, \ldots \tag{2.64}$$

$$\|p_* - p_n\|_{H^h_2} \leq C_2 \delta^{1/4} + \theta^n \left\|p_{\min,\lambda(\delta)} - p_0\right\|_{H^h_2}, \ n = 1, 2, \ldots \tag{2.65}$$

$$\|c_* - c_n\|_{L^h_2(\Omega_h)} \leq C_2 \delta^{1/4} + \theta^n \left\|p_{\min,\lambda(\delta)} - p_0\right\|_{H^h_2}, \ n = 1, 2, \ldots \tag{2.66}$$

where $\theta \in (0,1)$ *is the number of Theorem 2.4 and functions* $c_{\min,\lambda(\delta)}(\mathbf{x})$ *and* $c_n(\mathbf{x})$ *is reconstructed from functions* $p_{\min,\lambda(\delta)}$ *and* $p_n(\mathbf{x}, k)$ *respectively using (2.19)–(2.21) and (2.50).*

Remark 2.2. *Since* $R > 0$ *and* $p_0 \in B(R)$ *are chosen arbitrarily, then Theorem 2.5 ensures the* ***global convergence*** *of the gradient projection method for our case, see Abstract and section 1 for our definition of global convergence.*

3 Convexification for Backscattering Experimental Data for Buried Mine-like and IED-like Targets [12]

We present in this section a numerical study of the application of our convexification method to microwave experimental backscatter data for buried mine-like and IED-like targets [12]. One of possible applications is in the standoff detection of explosives. We note that these data were treated in [8] by the tail functions globally convergent method. We first describe very briefly the measured data and its preprocessing which is important for the application of our convexification method. We refer to [8] for all the details of data collection and preprocessing.

3.1 Measured data

The experimental data were measured by a scattering facility at the University of North Carolina at Charlotte. We have measured the backscatter data for objects buried in a sandbox. This sandbox was filled with dry sand and contains no moisture, see Figures 1. The data were measured on a rectangular surface of dimensions 1 m $\times$ 1 m. The distance between this surface and the sandbox was about 75 centimeters (cm). The coordinate system is chosen in such a way that the $x-$axis and the $y-$axis are respectively the horizontal and the vertical axis, while the $z-$axis is orthogonal to the measurement surface. The direction from the measurement surface to the target is the positive direction of the $z-$axis.

The measurements consist of multi-frequency backscatter data associated with 300 frequency points uniformly distributed over the range from 1 GHz to 10 GHz. However, we work with the preprocessed data which are stable on narrow intervals of frequencies centered at 2.6 GHz, 3.01 GHz or 3.1 GHz. Since the corresponding wavelength for 2.6 GHz is 11.5 cm, the distance between the source and the buried targets was about at least 6.17 wavelengths. This distance is sufficiently large in terms of wavelengths, and therefore justifies our modeling of the source as a plane wave. The backscatter data were generated by a single direction of the incident plane wave.

These experimental data were preprocessed in [8]. So, we present here the performance of our inversion method on that preprocessed data instead of the raw ones. The preprocessing developed in the cited paper comprises two main goals: distill the signals reflected by our buried targets from signals reflected by the sandbox and other unwanted objects, and reduce the noise in the data as well as the computational domain.

For the convenience of the readers We now briefly summarize the main steps of the data preprocessing developed in [8]:

Step 1. Subtract the reference data from the measured data for buried objects. The reference data are the ones measured in the case when the sandbox contains no buried objects. This subtraction helps us to sort of extract the signals of the buried targets from the total signal and also to reduce the noise.

Step 2. The data obtained after Step 1 were back propagated to the sandbox using the data propagation process. This process aims to "move" the data closer to the target. As a result, we obtain reasonable estimates for the location of the buried targets, particularly in the $(x, y)-$plane, see Figure 2. In addition, this step helps us reduce the computational domain.

Step 3. Determine an interval of frequencies on which the data obtained after Step 2 are stable.

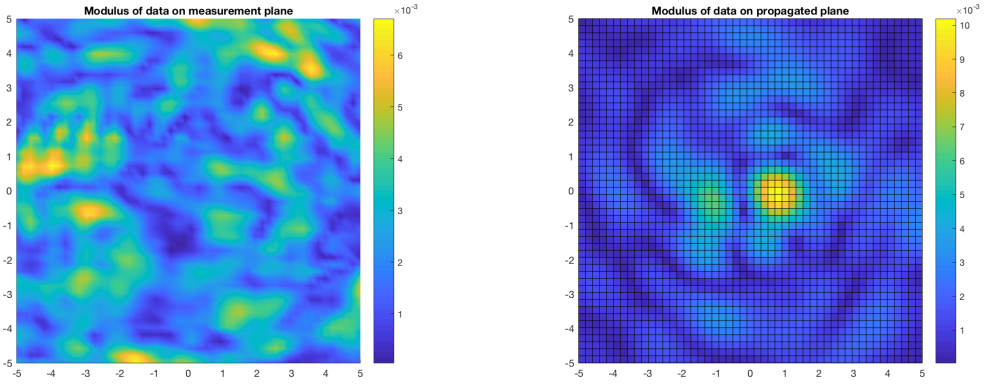

(a) (b)

Figure 2: *a) Absolute value of measured experimental data for the buried target 4 (sycamore, see table 1). b) Absolute value of the propagated data of a). Comparison of a) and b) clearly shows how useful the data propagation procedure is.*

3.2 Reconstruction results

We present in this section the results of reconstructions from experimental data for the objects buried in a sandbox in Table 1 using our convexification method.

In Table 2 we present the optimal frequencies and corresponding intervals of wavenumbers $[\underline{k}, \overline{k}]$ for our objects. We refer to [8] for the details of the determination of these intervals.

The objects with their directly measured dielectric constant c_{meas} and computed coefficient c_{comp} along with corresponding measurement ε_{meas} and computational errors $\varepsilon_{comp} = |c_{comp} - c_{meas}|/c_{meas} * 100\%$ are listed in Table 3. Note that the coefficients c_{comp} in Table 3 are the maximal values of the reconstructed functions $c(\mathbf{x})$. In all our numerical tests we have used reasonable values of parameters $\mu = \lambda = 3.0$.

Considering the significant amount of noise in the measured data, the computational errors ε_{comp} of reconstructed coefficients are sufficiently small. The computed dielectric constant of object 3 (a piece of rock) has the biggest error $\varepsilon_{comp} = 9.63\%$, but it is lower than its measurement error 21.3%.

Table 1: Buried objects

Number	Description	Size in $x \times y \times z$ directions (in cm)
1	Bamboo	$3.8 \times 11.6 \times 3.8$
2	Geode	$8.8 \times 8.8 \times 8.8$
3	Rock	$10.5 \times 7.5 \times 4.0$
4	Sycamore	$3.8 \times 9.9 \times 3.8$
5	Wet wood	$9.1 \times 5.7 \times 5.8$
6	Yellow pine	$9.0 \times 8.3 \times 5.8$

In Table 4 we present estimated locations of objects and locations of the reconstructed objects, i.e. the location of the maximum value of computed coefficient $\max(c_{comp}(\mathbf{x}))$. Errors of locations are small comparable with the size of the computational domain where we solve our inverse problem.

3.3 Conclusions

In our computations we have used the following parameter λ, which was found by trial and error:

$$\lambda = 3. \tag{3.1}$$

This means that even though theorems 2.1-2.5 are valid for sufficiently large values of λ, in computations one can choose reasonably values of λ.

Table 3 and Figures 3, 4 demonstrate that our numerical method accurately reconstructs both dielectric constants and locations of targets in **THE MOST CHALLENGING CASE** of backscattering experimental data collected for buried targets.

Table 2: Optimal frequencies and interval of wavenumbers

Number	Optimal frequency, GHz	Interval of wavenumbers $[\underline{k}, \overline{k}]$
1	3.10	[6.322, 6.638]
2	3.01	[6.133, 6.448]
3	3.01	[6.070, 6.385]
4	3.10	[6.322, 6.638]
5	2.62	[5.313, 5.691]
6	2.62	[5.313, 5.691]

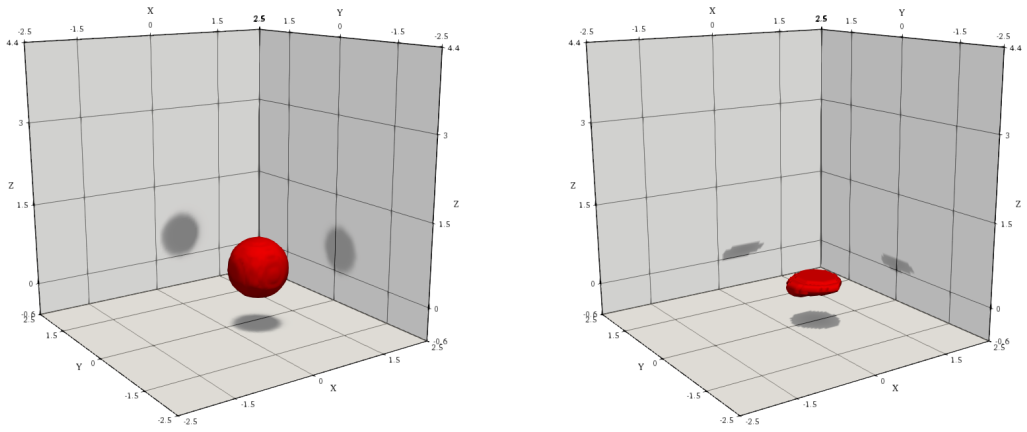

(a) (b)

Figure 3: *Reconstruction result for target number 2 (Table 1): (a) exact image, (b) computed image. One can see that the location of the target is imaged accurately (also, see Table 4). The dielectric constant of the target is also accurately imaged (also, see Table 3).*

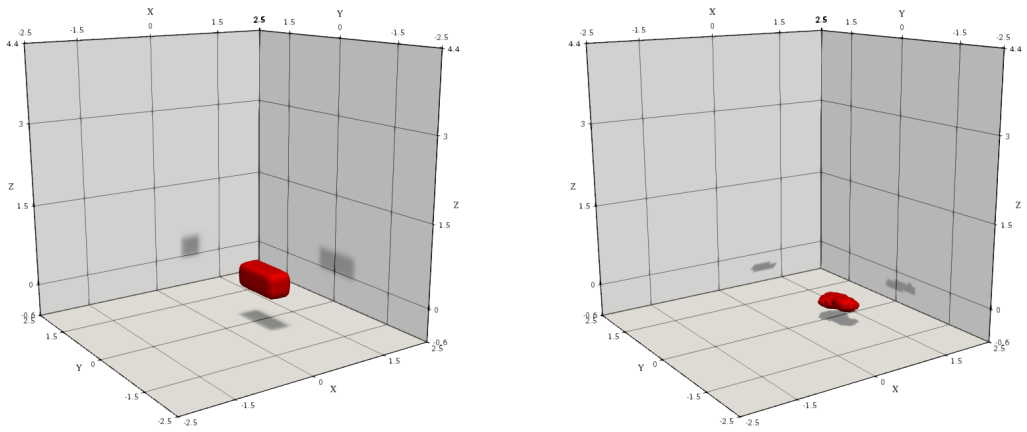

(a) (b)

Figure 4: *Reconstruction result for target number 4 (Table 1): (a) exact image, (b) computed image. One can see that the location of the target is imaged accurately (also, see Table 4). The dielectric constant of the target is also accurately imaged (also, see Table 3).*

Table 3: Measured and reconstructed coefficients of objects

Number	c_{meas}	ε_{meas}	c_{comp}	ε_{comp}
1	4.50	5.99%	4.69	4.22%
2	5.45	1.13%	5.28	3.12%
3	5.61	21.3%	5.07	9.63%
4	4.89	2.89%	4.95	1.23%
5	7.58	4.69%	8.06	6.33%
6	4.89	1.54%	5.22	8.75%

Table 4: Estimated and reconstructed locations of objects

Number	Estimated location in (x, y, z)	Computed location in (x, y, z)
1	(0.80, -0.11, 0.19)	(0.83, 0.03, -0.05)
2	(0.58, -0.14, 0.44)	(0.63, 0.03, 0.16)
3	(0.62, -0.14, 0.20)	(0.63, 0.08, -0.20)
4	(0.80, -0.04, 0.19)	(1.04, 0.08, -0.30)
5	(0.57, -0.42, 0.29)	(0.53, -0.08, 0.16)
6	(0.54, -0.33, 0.29)	(0.53, -0.03, 0.21)

4 Collaboration with Engineers from the US Army Research Laboratory

Since 2012 the PI very fruitfully collaborates with engineers from the US Army Research Laboratory, Drs. Lam Nguyen and Anders Sullivan. This collaboration has been supported by ARO grants W911NF-11-1-0399 and W911NF-15-1-0233. The PI has total five (5) joint publications with these people [6, 15, 32, 34, 35] and one joint paper [14] was recently submitted. The support of ARO is acknowledged in all of these. During this reportage period the paper [6] was published and the paper [14] was submitted.

The radar community is currently relying only on the energy information of radar images, see, e.g. [46]. Unlike this, in our papers with ARL engineers, we compute estimates of dielectric constants of targets. Our hope is that these estimates might help in the future to develop new classification procedures, which would combine the currently used energy information with the estimates of dielectric constants. This combination, in turn might result in lower false alarm rates. Our targets are three dimensional ones of course. On the other hand, that radar can measure only one time dependent curve for each target. Thus, what can be done at most by any data inversion technique is to estimate a sort of an average of the dielectric constant for a target. We believe, however, that even these estimates might

be useful for the goal of decreasing the false alarm rate. Thus, we model the wave propagation process by the 1-D Helmholtz equation.

In this collaboration, the role of the PI is to apply his globally convergent numerical methods to the experimental data collected by the Forward Looking Radar of ARL, see [41] for a description of this radar. We point out that those experimental ARL data were collected in the field, as opposed to the data collected in a laboratory of previous sections. The environment was quite cluttered one, which makes our imaging goal much more challenging.

In the previous annual report to ARO [23] a description of applications to the ARL data of the 1-D version of the convexification globally convergent numerical method was described. The corresponding joint paper with L. Nguyen and A. Sullivan is published during the reportage period [6].

However, in this section we show how a new version of the convexification method works for the ARL data. We follow our recently submitted paper [14], which is again joint with L. Nguyen and A. Sullivan. In fact, this version is a modification of the new approach to the convexification of the PI [7]. The analytical paper [7] of the PI shows how to apply the convexification in the case when the point source moves along an interval of a straight line, also see section 6. Unlike [7], we now have a moving frequency and adapt the idea of [7] to this case.

The convexification method of this section has the following two important new features, compared with the one of section 2 as well as with the 1-D version of [6] of the method of section 2:

1. Most importantly, we do not work here with a nonlinear integro differential equation in which the integration is carried out with respect to the wave number. This enables us to avoid the use of the use of the tail function.

2. We do not need to work here with large values of wave numbers.

4.1 Statement of the inverse problem

Let the function $c(x), x \in \mathbb{R}$ be the spatially distributed dielectric constant of the medium. We assume that

$$c \in C^2(\mathbb{R}), c(x) \geq 1, \forall x \in \mathbb{R}, \tag{4.1}$$

$$c(x) = 1, \forall x \notin (0,1). \tag{4.2}$$

Fix the source position $x_0 < 0$. For brevity, we do not indicate below dependence of our functions on x_0. Consider the 1-D Helmholtz equation for the function $u(x,k)$,

$$u'' + k^2 c(x) u = -\delta(x - x_0), x \in \mathbb{R}, \tag{4.3}$$

$$\lim_{x \to \infty} (u' + iku) = 0, \lim_{x \to -\infty} (u' - iku) = 0. \tag{4.4}$$

Let $u_0(x,k)$ be the solution of the problem (4.3), (4.4) for the case $c(x) \equiv 1$. Then

$$u_0(x,k) = \frac{\exp(-ik|x - x_0|)}{2ik}. \tag{4.5}$$

Our interest is in the following inverse problem:

Coefficient Inverse Scattering Problem (CISP). *Let* $[\underline{k},\overline{k}] \subset (0,\infty)$ *be an interval of wavenumbers* k. *Reconstruct the function* $c(x)$, *assuming that the following function* $g_0(k)$ *is known*

$$g_0(k) = \frac{u(0,k)}{u_0(0,k)}, k \in [\underline{k},\overline{k}]. \tag{4.6}$$

Denote

$$w(x,k) = \frac{u(x,k)}{u_0(x,k)}. \tag{4.7}$$

It follows from (4.6), (4.7) and [15] that

$$w(0,k) = g_0(k), k \in [\underline{k},\overline{k}], \tag{4.8}$$

$$w'(0,k) = g_1(k) = 2ik(g_0(k)-1), k \in [\underline{k},\overline{k}]. \tag{4.9}$$

It was shown in [15], in the previous annual report [23] and in section 2.2.1 how to uniquely define $\log w(x,k)$.

4.2 A special orthonormal basis in $L_2\left(\underline{k},\overline{k}\right)$

This basis was first constructed by the PI in [7]. In this reference, functions of that basis are dependent on the position of the point source, and this source runs along an interval of a straight line. We now briefly repeat that construction for the case when these functions depend on the wave number k. The latter is a new idea.

Let $(,)$ denotes the scalar product in $L_2\left(\underline{k},\overline{k}\right)$. We need to construct an orthonormal basis $\{\psi_n(k)\}_{n=0}^{\infty}$ of real valued function in the space $L_2\left(\underline{k},\overline{k}\right)$ such that the following two conditions are met:

1. $\psi_n \in C^1\left[\underline{k},\overline{k}\right], \forall n = 0,1,...$
2. Let $a_{mn} = (\psi_n', \psi_m)$. Then the matrix $M_N = (a_{mn})_{m,n=0}^{N-1}$ is invertible for any $N = 1,2,...$

Neither classical orthonormal polynomials nor the basis of trigonometric functions

$$\left\{\exp\left[in\pi\left(k-\underline{k}\right)/\left(\overline{k}-\underline{k}\right)\right]\right\}_{n=0}^{\infty}$$

do not satisfy the second condition. This is because in any of these two cases the first column of the matrix M_N would be equal to zero.

Consider the set of functions $\left\{k^n e^k\right\}_{n=0}^{\infty}$. This set is complete in $L_2(0,1)$. We orthonormalize it using the classical Gram-Schmidt orthonormalization procedure. We start from $n=0$, then take $n=1$, etc. Then we obtain the orthonormal basis $\{\varphi_n(k)\}_{n=0}^{\infty}$ in $L_2(0,1)$. Each function $\varphi_n(k)$ has the form

$$\varphi_n(k) = p_n(k)\, e^k,$$

where $p_n(k)$ is the polynomial of the degree n. Next, we set

$$\psi_n(k) = \frac{1}{\sqrt{\overline{k}-\underline{k}}}\varphi_n\left(\frac{k-\underline{k}}{\overline{k}-\underline{k}}\right).$$

Thus, the set $\{\psi_n(k)\}_{n=0}^{\infty}$ is an orthonormal basis in the space $L_2\left(\underline{k},\overline{k}\right)$. Lemma 4.1 ensures that the above property number 2 holds for functions $\psi_n(k)$.

Lemma 4.1 [7]. *Denote* $a_{mn} = (\psi_n', \psi_m)$. *Then*

$$a_{mn} = \begin{cases} \left(\overline{k}-\underline{k}\right)^{-1} \text{ if } n = m, \\ 0 \text{ if } n < m. \end{cases} \tag{4.10}$$

For an integer $N \geq 1$ *consider the* $N \times N$ *matrix* $M_N = (a_{mn})_{(m,n)=(0,0)}^{(N-1,N-1)}$. *Then (4.10) implies that* M_N *is an upper diagonal matrix with* $\det(M_N) = \left(\overline{k}-\underline{k}\right)^{-N} \neq 0$. *Thus, the inverse matrix* M_N^{-1} *exists.*

4.3 A system of coupled quasilinear ordinary differential equations

Let $\log w(x,k)$ be the function constructed in (4.7). Consider the function

$$v(x,k) = \frac{\log w(x,k)}{k^2}, \quad x \in [0,1],\ k \in \left[\underline{k},\overline{k}\right]. \tag{4.11}$$

Substitution in equation (4.3) leads to

$$v'' + k^2\left(v'\right)^2 - 2ikv' = 1 - c(x) = -\beta(x), \quad x \in [0,1],\ k \in \left[\underline{k},\overline{k}\right]. \tag{4.12}$$

Also, by (4.7)-(4.9)

$$v(0,k) = q_0(k), \quad v'(0,k) = q_1(k), \tag{4.13}$$

where

$$q_0(k) = \frac{\log g_0(k)}{k^2}, \quad q_1(k) = \frac{g_1(k)}{g_0(k)\,k^2}. \tag{4.14}$$

In addition, (4.2) and (4.11) imply that

$$v'(1,k) = 0. \tag{4.15}$$

Differentiate both sides of equation (4.12) with respect to k and use the fact that $\partial_k(1-c(x)) = 0$. We obtain

$$v_k'' + 2k^2 v_k' v' + 2k\left(v'\right)^2 - 2ikv_k' - 2iv' = 0. \tag{4.16}$$

We now assume that the function $v(x,k)$ can be represented via a truncated Fourier series with respect to the orthonormal basis $\{\psi_n(k)\}_{n=0}^{\infty}$. In fact, this is our main approximation. Thus, for an integer $N \geq 1$, we assume that

$$v(x,k) = \sum_{n=0}^{N-1} y_n(x)\,\psi_n(k) \tag{4.17}$$

for $x \in [0,1], k \in \left[\underline{k}, \overline{k}\right]$. Here coefficients $y_n(x)$ of the expansion (4.19) are unknown and should be determined as the main part of the solution of our CISP. In particular, (4.12) and (4.17) imply that

$$c(x) = 1 - \sum_{n=0}^{N-1} y_n''(x)\psi_n(k) - k^2\left(\sum_{n=0}^{N-1} y_n'(x)\psi_n(k)\right)^2 \tag{4.18}$$

$$+2ik\sum_{n=0}^{N-1} y_n'(x)\psi_n(k).$$

Substituting (4.17) in (4.16), we obtain

$$\sum_{n=0}^{N-1} y_n''(x)\psi_n'(k) + 2k^2\sum_{n,m=0}^{N-1} y_n'(x)y_m'(x)\psi_n'(k)\psi_m'(k)$$

$$+ 2k\left[\sum_{n=0}^{N-1} y_n'(x)\psi_n(k)\right]^2 - 2ik\sum_{n=0}^{N-1} y_n'(x)\psi_n'(k) \tag{4.19}$$

$$-2i\sum_{n=0}^{N-1} y_n'(x)\psi_n(k) = 0.$$

Introduce the $N-$D vector function $y(x)$,

$$y(x) = (y_0, ..., y_{N-1})^T(x). \tag{4.20}$$

Let $s \in [0, N-1]$ be an integer. Multiply both sides of (6.21) by $\psi_s(k)$ and integrate with respect to $k \in \left(\underline{k}, \overline{k}\right)$. We obtain

$$M_N y'' + \widetilde{F}(y') = 0, \quad x \in [0,1]. \tag{4.21}$$

Here the vector function $\widetilde{F}(\cdot)$ is quadratic with respect to the functions $y_n'(x)$. Since by Lemma 3.1 the matrix M_N is invertible, we multiply both sides of (2.51) by M_N^{-1} and obtain

$$y'' + F(y') = 0, \quad x \in [0,1], \tag{4.22}$$

where the vector function $F(y') = M_N^{-1}\widetilde{F}(y')$. Therefore, the vector function $F(y')$ is quadratic with respect to the functions $y_n'(x)$. In addition, (4.13) and (4.15) imply that the vector function $y(x)$ satisfies the following boundary conditions:

$$y(0) = f_0, \quad y'(0) = f_1, \quad y'(1) = 0. \tag{4.23}$$

Note that due to the boundary condition $y'(1) = 0$, (4.22), (4.23) is not the regular Cauchy problem for the system (4.22) of coupled quasilinear Ordinary Differential Equations. Thus,

our effort below is focused on the numerical solution of the problem (4.22), (4.23). Indeed, if we would solve it, then, using (2.47) and (4.20), we would find the target coefficient $c(x)$. We solve this problem via minimizing our weighted Tikhonov-like functional with the CWF. First, we formulate the Carleman estimate for the operator d^2/dx^2.

Lemma 4.2 (Carleman estimate) [15]. *For any complex valued function $u \in H^2(0,1)$ with $u(0) = u'(0) = 0$ and for any parameter $\lambda \geq 1$ the following Carleman estimate holds*

$$\int_0^1 |u''|^2 e^{-2\lambda x} dx \geq C \int_0^1 |u''|^2 e^{-2\lambda x} dx + C \left[\lambda \int_0^1 |u'|^2 e^{-2\lambda x} dx + \lambda^3 \int_0^1 |u|^2 e^{-2\lambda x} dx \right],$$

where the constant $C > 0$ is independent on u and λ.

Remark 4.1. *Using Lemma 4.2 as well as arguments, which are completely similar with those of the proof of Theorem 3.1 of [7], one can prove that there exists at most one solution $V \in H^2(0,1)$ of the problem (4.22), (4.23).*

4.4 Globally strictly convex weighted Tikhonov-like functional

Introduce the cut-off function $\chi(x)$,

$$\chi \in C^2[0,1], \quad \chi(x) = \begin{cases} 1, x \in [0,1/2], \\ 0, x \in [3/4,1], \\ \in (0,1), x \in (1/2,3/4). \end{cases} \tag{4.24}$$

Consider the $N-$D vector function $f(x)$ defined as

$$f(x) = [f_0 + x f_1] \chi(x). \tag{4.25}$$

Then

$$f \in C^2[0,1], \quad f(0) = f_0, \quad f'(0) = f_1, \quad f'(1) = 0.$$

Hence

$$(y - f)(0) = 0, \quad (y - f)'(0) = 0, \quad (y - f)'(1) = 0.$$

Let $R > 0$ be an arbitrary number. Consider the sets $B(R, f_0, f_1)$ and $B_0(R)$ of $N-$D vector functions $W(x)$ and $p(x)$ defined as:

$$B(R, f_0, f_1) = \left\{ \begin{array}{c} W \in H^2(0,1): \\ W(0) = f_0, W'(0) = f_1, W'(1) = 0, \\ \|W - f\|_{H^2(0,1)} < R \end{array} \right\}, \tag{4.26}$$

$$B_0(R) = \left\{ p \in H^2(0,1) : p(0) = p'(0) = p'(1) = 0, \|p\|_{H^2(0,1)} < R \right\}. \tag{4.27}$$

Hence, all vector functions belonging to the set $B(R, f_0, f_1)$ satisfy boundary conditions (4.23). Note that both sets $B(R, f_0, f_1)$ and $B_0(R)$ are convex. The proof of Proposition 3.1 follows immediately from (4.26) and (4.27).

Proposition 4.1. *Let $f(x)$ be the vector function defined in (4.25). Then for any vector function $W \in B(R, f_0, f_1)$ the vector function $(W - f) \in B_0(R)$. And vice versa: for any vector function $p \in B_0(R)$ the vector function $(p + f) \in B(R, f_0, f_1)$.*

In accordance with the Tikhonov concept for ill-posed problems [48], we assume that there exists the exact solution y^* of the problem (4.22), (4.23) with the exact (i.e. noiseless) data

$$y^*(0) = f_0^*, \quad y^{*\prime}(0) = f_1^* \tag{4.28}$$

in (4.23) and $y^* \in B(R, f_0^*, f_1^*)$. Let a sufficiently small number $\delta \in (0, 1)$ represents the level of the noise in the data, i.e.

$$|f_0 - f_0^*| < \delta, \quad |f_1 - f_1^*| < \delta. \tag{4.29}$$

Similarly with (4.25) introduce the function $f^*(x)$,

$$f^*(x) = [f_0^* + x f_1^*] \chi(x). \tag{4.30}$$

It follows from (4.24), (4.25), (6.7) and (4.30) that

$$\|f - f^*\|_{C^2[0,1]} \leq B\delta. \tag{4.31}$$

Here and below $B = B(\chi) > 0$ denotes different positive numbers depending only on the function $\chi(x)$. Since δ is sufficiently small, we indicate below dependencies of some constants on f^* rather than on f.

Let $\alpha \in (0, 1)$ be the regularization parameter. Our Tikhonov-like weighted functional is

$$J_{\lambda,\alpha}(y) = e^{2\lambda} \int_0^1 |y'' + F(y')|^2 e^{-2\lambda x} dx + \alpha \|y\|^2_{H^2(0,1)}. \tag{4.32}$$

Here the multiplier $e^{2\lambda}$ is introduced to balance two terms in the right hand side of (4.32). We consider the following minimization problem:

Minimization Problem 3. *Minimize the functional $J_{\lambda,\alpha}(y)$ on the set $y \in \overline{B(R, f_0, f_1)}$.*

Remark 4.2. *In principle, estimate (4.33) of Theorem 5.1 tells one that it is not necessary to incorporate the regularization term $\alpha \|y\|^2_{H^2(0,1)}$ in the functional $J_{\lambda,\alpha}(y)$. Nevertheless we have observed in our computations that the presence of this term improves numerical results. This is why we introduce it here. The PI cannot yet explain the reason of this improvement.*

4.5 Global convergence theorems

In this section we formulate theorems about the functional $J_{\lambda,\alpha}(y)$. Theorem 5.1 is the central result of this section as well as of the paper [14]. Below $C_1 = C_1(R, F, N) > 0$ and $C_2 = C_2(R, F, N, \chi, f^*) > 0$ denote different numbers depending only on listed parameters.

Theorem 4.1. *The functional $J_{\lambda,\alpha}(y)$ has the Frechét derivative $J'_{\lambda,\alpha}(y)$ at each point $y \in B(2R, f_0, f_1)$. Also, there exists a number $\lambda_1 = \lambda_1(R, F, N) > 1$ depending only on listed parameters such that for all $\lambda \geq \lambda_1$ the functional $J_{\lambda,\alpha}(y)$ is strictly convex on the set $\overline{B(R, f_0, f_1)}$, i.e. for all $y_{(1)}, y_{(2)} \in \overline{B(R, f_0, f_1)}$*

$$J_{\lambda,\alpha}\left(y_{(2)}\right) - J_{\lambda,\alpha}\left(y_{(1)}\right) - J'_{\lambda,\alpha}\left(y_{(1)}\right)\left(y_{(2)} - y_{(1)}\right) \geq C_1 \left\|y_{(2)} - y_{(1)}\right\|^2_{H^2(0,1)}. \tag{4.33}$$

Corollary 4.1. *Consider the functional*

$$\Phi_{\lambda,\alpha}(p) = J_{\lambda,\alpha}(p + f), \quad \forall p \in \overline{B_0(R)}. \tag{4.34}$$

Then a direct analog of Theorem 4.1 is valid for this functional. More precisely, the functional $\Phi_{\lambda,\alpha}(P)$ has the Frechét derivative $\Phi'_{\lambda,\alpha}(p)$ at each point $p \in B_0(2R)$. Let $\lambda_1 = \lambda_1(R, F, N) > 1$ be the number of Theorem 5.1. Then there exists a number $\lambda_2 = \lambda_2(R, F, N, \chi, f^*) \geq \lambda_1$ depending only on listed parameters such that for all $\lambda \geq \lambda_2$ the functional $\Phi_{\lambda,\alpha}(p)$ is strictly convex on the set $\overline{B_0(R)}$, i.e. for all $p_1, p_2 \in \overline{B_0(R)}$

$$\Phi_{\lambda,\alpha}(p_2) - \Phi_{\lambda,\alpha}(p_1) - \Phi'_{\lambda,\alpha}(p_1)(p_2 - p_1) \geq C_2 \|p_2 - p_1\|^2_{H^2(0,1)}.$$

Theorem 4.2. *Let $\lambda_1 = \lambda_1(R, F, N) > 1$ and $\lambda_2 = \lambda_2(R, F, N, \chi, f^*) \geq \lambda_1$ be the numbers of Theorem 4.1 and Corollary 4.1 respectively. Let $f(x)$ be the function defined in (4.24), (4.25). Then for any $\lambda \geq \lambda_2$ and for any $\alpha \in (0,1)$ there exists a unique minimizer $y_{\min,\lambda,\alpha}$ of the functional $J_{\lambda,\alpha}(y)$ on the set $\overline{B(R, f_0, f_1)}$. In addition, for these values of λ and α there exists unique minimizer $p_{\min,\lambda,\alpha}$ of the functional $\Phi_{\lambda,\alpha}(p)$ on the set $\overline{B_0(R)}$. Furthermore, $p_{\min,\lambda,\alpha} = y_{\min,\lambda,\alpha} - f$ and*

$$\Phi'_{\lambda,\alpha}(p_{\min,\lambda,\alpha})(p_{\min,\lambda,\alpha} - p) \leq 0, \quad \forall p \in \overline{B_0(R)}, \tag{4.35}$$

$$J'_{\lambda,\alpha}(y_{\min,\lambda,\alpha})(y_{\min,\lambda,\alpha} - y) \leq 0, \quad \forall y \in \overline{B(R, f_0, f_1)}. \tag{4.36}$$

Theorem 4.3 (accuracy estimate). *Assume that the exact solution y^* of the problem (4.22), (4.23) exists and $y^* \in B(R, f_0^*, f_1^*)$. Also, assume that (6.15) and (6.7) hold. Denote $p^* = y^* - f^* \in B_0(R)$. In addition, assume that there exists the exact solution $c^*(x)$ of our CIP and this function satisfies conditions (4.1), (4.2). Suppose that the function $c^*(x)$ can be found from the vector function $y^*(x)$ via formula (4.18) in which functions y_n are replaced with components y_n^* of the vector function $y^*(x)$. Let $\lambda_1 = \lambda_1(R, F, N) > 1$ and $\lambda_2 = \lambda_2(R, F, N, \chi, f^*) \geq \lambda_1$ be the numbers of Theorem 4.1 and Corollary 4.1 respectively. Consider the number δ_0 such that $\delta_0 \in \left(0, e^{-4\lambda_2}\right)$. For any $\delta \in (0, \delta_0)$ we set $\lambda = \lambda(\delta) = \ln\left(\delta^{-1/4}\right) > \lambda_2$ and $\alpha = \alpha(\delta) = \sqrt{\delta}$. Let $y_{\min,\lambda,\alpha} \in B(R, f_0, f_1)$ and $p_{\min,\lambda,\alpha} = y_{\min,\lambda,\alpha} - f \in B_0(R)$ be the unique minimizers of the functionals $J_{\lambda,\alpha}(V)$ and $\Phi_{\lambda,\alpha}(p)$ on sets $B(R, f_0, f_1)$ and $B_0(R)$ respectively (Theorem 4.3). Then the following accuracy estimates hold:*

$$\|p_{\min,\lambda,\alpha} - p^*\|_{H^2(0,1)} \leq C_2 \delta^{1/4}, \tag{4.37}$$

$$\left\|y_{\min,\lambda(\delta),\alpha(\delta)} - y^*\right\|_{H^2(0,1)} \leq C_2\delta^{1/4}, \tag{4.38}$$

$$\left\|c_{\min,\lambda(\delta),\alpha(\delta)} - c^*\right\|_{L_2(0,1)} \leq C_2\delta^{1/4}, \tag{4.39}$$

where the function $c_{\min,\lambda(\delta),\alpha(\delta)}$ *is found from components* $y_{n,\min,\lambda(\delta),\alpha(\delta)}$ *of the vector function* $y_{\min,\lambda(\delta),\alpha(\delta)}$ *via formula (4.18).*

Define the subspace $H_0^2(0,1)$ of the space $H^2(0,1)$ as

$$H_0^2(0,1) = \left\{w \in H^2(0,1) : w(0) = w'(0) = w'(1) = 0\right\}.$$

By (4.27) $B_0(R) \subset H_0^2(0,1)$. Let $Q_{\overline{B_0}} : H_0^2(0,1) \to \overline{B_0(R)}$ be the projection operator of the space $H_0^2(0,1)$ on the closed ball $\overline{B_0(R)}$. Consider now the gradient projection method of the minimization of the functional (4.34) on the set $\overline{B_0(R)}$. Let $p_0 \in B_0(R)$ be an arbitrary point and $\gamma > 0$ be a number. We consider the following sequence:

$$p_n = Q_{\overline{B_0}}\left(p_{n-1} - \gamma\Phi'_{\lambda,\alpha}(p_{n-1})\right), \quad n = 1, 2, ... \tag{4.40}$$

Theorem 4.4 (global convergence of the gradient projection method). *Let conditions of Theorem 4.4 about exact solutions* y^* *and* c^* *hold. Let the numbers* $\lambda_1, \lambda_2, \delta, \lambda(\delta), \alpha(\delta)$ *be the same as in Theorem 4.4. Let an arbitrary point* $p_0 \in B_0(R)$ *be the starting point of the gradient projection method (4.40). Consider the sequence (4.40) and denote* $y^n = p_n + f$. *Then there exists a number* $\gamma_0 = \gamma_0(R, F, N, \chi, f^*, \delta) \in (0,1)$ *depending only on listed parameters such that for any* $\gamma \in (0, \gamma_0)$ *there exists a number* $s = s(\gamma) \in (0,1)$ such that *the following convergence estimates are valid:*

$$\left\|p_n - p_{\min,\lambda(\delta),\alpha(\delta)}\right\|_{H^2(0,1)} \leq s^n \left\|p_0 - p_{\min,\lambda(\delta),\alpha(\delta)}\right\|_{H^2(0,1)}, \; n = 1, 2, ..., \tag{4.41}$$

$$\left\|y^n - y_{\min,\lambda(\delta),\alpha(\delta)}\right\|_{H^2(0,1)} \leq s^n \left\|y^0 - y_{\min,\lambda(\delta),\alpha(\delta)}\right\|_{H^2(0,1)}, \; n = 1, 2, ..., \tag{4.42}$$

$$\left\|y^n - y^*\right\|_{H^2(0,1)} \leq C_2\delta^{1/4} + s^n \left\|y^0 - y_{\min,\lambda(\delta),\alpha(\delta)}\right\|_{H^2(0,1)}, \; n = 1, 2, ..., \tag{4.43}$$

$$\left\|c^n - c^*\right\|_{L_2(0,1)} \leq C_2\delta^{1/4} + s^n \left\|y^0 - y_{\min,\lambda(\delta),\alpha(\delta)}\right\|_{H^2(0,1)}, \; n = 1, 2, ..., \tag{4.44}$$

where functions $c^n(x)$ *are found from components* $y_m^n, m = 0, ..., N-1$ *of vector functions* y^n *via formula (4.18).*

Remark 4.3. *Since* $R > 0$ *is an arbitrary number and* p_0 *is an arbitrary point of the ball* $B_0(R)$, *then Theorem 4.4 ensures the* ***global convergence*** *of the gradient projection method (4.40), see Abstract and section 1 for our definition of global convergence.*

4.6 Numerical studies of experimental data of US Army Research Laboratory

We generate the data for the forward problem (4.3), (4.4) via the numerical solution of the Lippmann Schwinger equation

$$u(x,k) = \frac{e^{-ik|x-x_0|}}{2ik} + \frac{k}{2i}\int\limits_0^1 e^{-ik|x-\xi|}\left(c(\xi) - 1\right)u(\xi,k)\,d\xi, \tag{4.45}$$

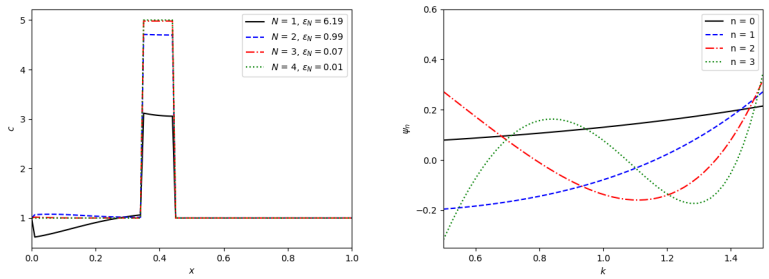

(a) (b)

Figure 5: *a) The approximate functions $c_{appr,N}(x)$, b) basis functions $\psi_n(k)$*

which is equivalent with the forward problem (4.3), (4.4).

4.6.1 The optimal number N terms in the expansion (4.17)

We need to determine the optimal number N of terms in the truncated Fourier series (4.17). To do this, we first solve the Lippmann-Schwinger equation (4.45) for a reference target with $c(x) := \widehat{c}_{true}(x)$. Next, we compute vector functions $y_{true,N}(x)$ in (4.17), (4.20) for different values of N and reconstruct approximate functions $c_{appr,N}(x)$ via (4.18). Figure 5a shows the functions $c_{appr,N}(x)$ for $N = 1, 2, 3, 4$, where $\widehat{c}_{true} = 5.0$ and $x_{loc} = 0.4$. The corresponding basis functions $\psi_n(k)$ are shown on Figure 5b. One can see that the functions $c_{true,N}(x)$ are accurately approximated for both $N = 3$ and $N = 4$, and their approximation errors $\varepsilon_N = \|c_{appr,N} - c_{true}\|_{L^2(0,1)}$ are sufficiently small: $\varepsilon_N = 0.07$ and 0.01, respectively. Therefore, we choose the optimal number of functions in our basis $N = 3$.

4.6.2 Numerical implementation

For the numerical solution we use the finite difference discretization method. So we divide the interval $x \in [0, 1]$ into N_x equal subintervals and obtain the mesh $x_j = jh_x$, $j = 0, \ldots, N_x$, $h_x = 1.0/N_x$. Combining this mesh with the mesh for wave numbers k_m, we obtain the $N_k \times N_x$ two dimensional mesh with the grid points (k_m, x_j). We need to find the discrete function $V = \{v_{m,j}\}$, where $v_{m,j} = v(k_m, x_j)$ are its values at those grid points. The discrete version of equation (4.17) can be written as

$$V = \Psi Y,$$

where $\Psi = \{\psi_{m,n}\}$ is the $N_k \times N$ matrix with $\psi_{m,n} = \psi_n(k_m)$ and $Y = \{y_{n,j}\}$ is the $N \times N_x$ two dimensional discrete vector function y (4.20).

The main objective of the proposed method is to find the minimizer of functional $J_{\lambda,\alpha}(y)$ (4.32). Naturally, we minimize this functional numerically for the case of the discrete function Y. The details of finite difference discretization of the functional and its gradient

are not described here for brevity. We refer to [33], where discretization of similar functional is performed analytically using the Kronecker delta function. Although, our theory suggest the gradient projection method for the minimization, we have noticed that the conjugate gradient method (CG) works well for our problem. This method is easier to implement numerically and it gives practically the same results as the gradient projection method. The latter has been consistently observed in the previous works on the numerical issues of the convexification method [1, 6, 12, 13, 14, 17, 18]. Also, to decrease the necessity of calculating the functional and its gradient on each iterative step, we have decided not to use the standard line search algorithm to seek the step size of the minimization process. Instead, we begin with the initial step size 10^{-7}. On each iteration, the step size is reduced 10 times for the next iteration if the value of the functional on the current iteration is greater than its value on the previous iteration. Otherwise, the step size remains the same for the next iteration. Also, after every 1000 iterations the step size is increased by 10 times. The minimization algorithm is stopped either after 15000 iterations or when the step size becomes less then 10^{-14}. The latter means that the functional can no longer decrease and its minimizer is reached.

4.6.3 Reconstruction results for experimental data

We have used in our computations the following parameters λ and α which we have found by trial and error:

$$\lambda = 3, \alpha = 0.05.$$

In particular, this means that even though theorems 4.1-4.4 are valid for sufficiently large values of λ, in computations one can choose reasonably values of λ.

Now we demonstrate the reconstruction results for the experimental data. Recall that these data were collected in the field (as opposed to a laboratory) by the Forward Looking Radar of the US Army Research Laboratory [41]. The scheme of the data collection is presented on Figure 6. Originally the backscattering time dependent data are measured, one time resolved curve for each target. To obtain the data in the frequency domain, we apply Fourier transform.

Targets of our interest were surrounded by cluttered environment, which is of course a complicating factor for their imaging. Horizontal coordinates of targets were provided by Ground Positioning System (GPS) with a good accuracy. As to the burial depths of targets, they are not of an interest in this specific application. In addition, we had the data for two targets located in air. Hence, the burial depth for these two makes no sense. Furthermore, it is clear from the descriptions of [32, 34, 35] of the data collection process that it is unlikely that an information about burial depths of buried targets can ever be extracted from these data. All what was known to us was that burial depths of targets buried in the ground (dry sand) was a few centimeters. With respect to our algorithm this means that we are not interested in the location of the target. Rather, our interest is in the target/background contrast in the dielectric constant, see (4.46) and (4.47).

We posses experimental data for five (5) targets. Our *a priori* information was that two

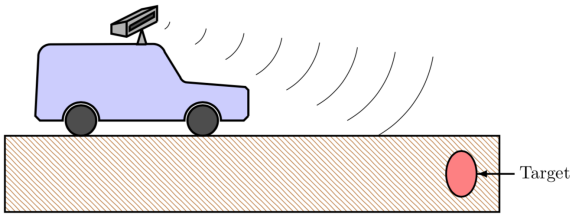

Figure 6: *Schematic diagram of data collection by the Forward Looking Radar of ARL.*

(2) targets, bush and a wood stake, were located in air, and three (3) targets, metallic box, metallic cylinder and plastic cylinder, were buried in a dry sand. We also knew that each experimental data set was collected for a single target only. We introduce the number c_{bg} for the dielectric constant of the background, which is $c_{bg} = 1.0$ if the target is in air, and $c_{bg} \in [3.0, 5.0]$ if the target is buried. Here we use values of the dielectric constant of dry sand, see tables [47] of dielectric constants. Consequently, the computed number

$$\widehat{c}_{comp} = \max c_{comp}(x)$$

is an estimation of the contrast between the target and the background $c_{contrast}$,

$$c_{contrast} = \frac{c_{target}}{c_{bg}} \approx \widehat{c}_{comp}. \tag{4.46}$$

where c_{target} is the true dielectric constant of the target.

Also, we know that the dielectric constant of plastic cylinder is less then the one of sand with $0 < c_{contrast} < 1.0$, see "plastic pellets" in [47]. Therefore, recalling that

$$\beta(\mathbf{x}) = c(\mathbf{x}) - 1,$$

we modify (4.46) for this case as:

$$c_{contrast} = \begin{cases} \mathrm{Re}(\beta_{comp}) + 1.0, & \text{if } \mathrm{Re}(\beta_{comp}) \leq \rho \min(\mathrm{Re}(\beta_{comp})), \\ 1.0, & \text{otherwise and also if } \mathrm{Re}(\beta_{comp}) < -1.0, \end{cases}$$

where $\rho = 0.5$. Here, the condition $\mathrm{Re}(\beta_{comp}) < -1.0$ must be applied before the truncation. Next, we introduce the number $\widehat{c}_{est}$, which is our estimation of the dielectric constant of the target,

$$\widehat{c}_{est} = c_{bg}\widehat{c}_{comp}, \tag{4.47}$$

where $\widehat{c}_{comp} = \min(c_{comp})$ for the plastic cylinder, and $\widehat{c}_{comp} = \max(c_{comp})$ for other targets. *A priori* differentiation between the plastic cylinder and other targets is performed prior our computations via an analysis of the data, see [34].

The numbers function $\widehat{c}_{comp}$ as well as estimates of dielectric constant $\widehat{c}_{est}$ via (4.47) for our targets are listed in Table 5. Since we did not measure dielectric constants of targets,

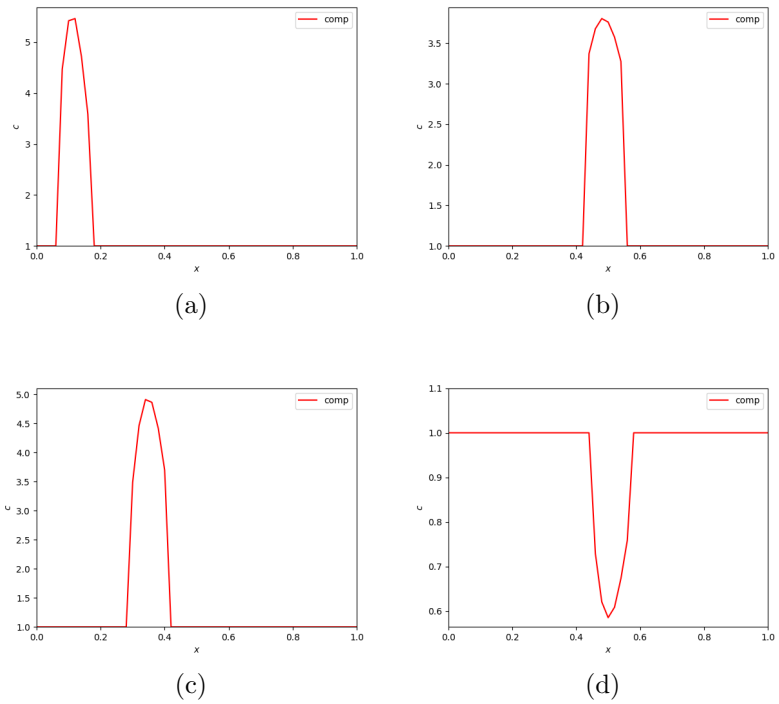

Figure 7: *Reconstruction results for: a) bush, b) wood stake, c) metallic box, d) plastic cylinder*

then the values of c_{target} were obtained from tables [47]. Also, it was shown in [34] that one can assign large values of dielectric constants to metallic targets as $c_{met} := c_{target} \in [10, 30]$. As to the bush, this target is considered as the hardest one to image since it is obviously a very heterogeneous one due to the presence of many leaves. We took for this case c_{target} from [28]. Our results are summarized in Table 5.

One can see that all values of estimated dielectric constants $\widehat{c}_{est}$ in this table are within tabulated limits. Given that dielectric constants of targets were not measured in experiments, Table 5 is a quite encouraging one for the engineers of ARL: Anders Sullivan and Lam Nguyen. Indeed, results presented in this table indicate that a future software based on the above algorithm might indeed provide rather accurate estimates of dielectric constants of targets of interest. An important additional point of the encouragement of engineers is that these results are obtained for targets surrounded by a realistic cluttered environment. Hence, engineers conjecture that an intriguing opportunity might occur in the future to decrease the false alarm rate. Certainly more comprehensive studies of large collections of experimental data sets are necessary to verify this conjecture.

Table 5: Reconstruction results for experimental targets.

Target	Air/Sand	$\widehat{c}_{contrast}$	c_{bg}	$\widehat{c}_{est}$	c_{target}
Bush	Air	5.47	1.0	5.47	$[3.0, 20.0]$
Wood stake	Air	3.80	1.0	3.80	$[2.0, 6.0]$
Metal box	Sand	4.91	$[3.0, 5.0]$	$[14.73, 24.55]$	$[10.0, 30.0]$
Metal cylinder	Sand	4.84	$[3.0, 5.0]$	$[14.52, 24.20]$	$[10.0, 30.0]$
Plastic cylinder	Sand	0.59	$[3.0, 5.0]$	$[1.77, 2.95]$	$[1.1, 3.2]$

5 Convexification for the Case of a Moving Point Source

In all previous works of the PI on globally convergent numerical methods for CISPs only the case of either a single position of a point source or a single direction of the incident plane wave was considered. In this section, however, we present a recent new idea of the PI on applying the convexification to the case when the point source is moving along an interval of a straight line [7]. The PI hopes that this idea might improve images of shapes of targets. A schematic diagram of imaging of land mines and IEDs using a moving point source and backscattering data is presented on Figure 8. In this section, we follow papers [7, 13].

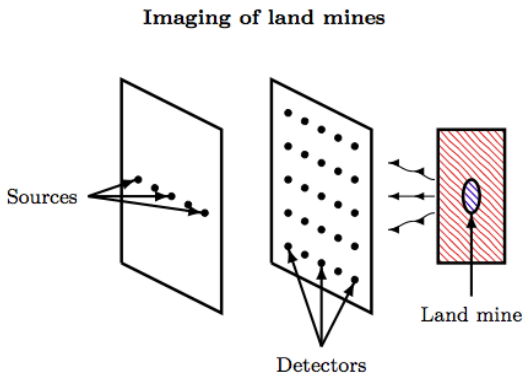

Figure 8: *A schematic diagram of measurements of backscattering data to image land mines and IEDs using a point source moving along an interval of a straight line.*

In particular, it is shown in this section that the classical and very popular inverse problem of Electrical Impedance Tomography (EIT) is solved numerically by this new version of the convexification method [13]. This is the *first* solution of this problem by a *globally convergent numerical method*.

5.1 A special orthonormal basis in $L_2(0,1)$

First, we construct a *new* orthonormal basis in the space $L_2(0,1)$ of functions depending on x_0 [7]. This basis is such that the first derivative with respect to x_0 of any element of this basis is not identically zero. In addition, this derivative should be a linear combination of a finite number of elements of this basis. Neither the basis of trigonometric functions nor the basis of standard orthonormal polynomials are not suitable for this goal. Therefore, we construct a new basis. Our basis is similar with Laguerre functions, which, however, form an orthonormal basis in $L_2(0,\infty)$ rather than in $L_2(0,1)$.

For $x_0 \in (0,1)$, consider the set of functions $\left\{x_0^k e^{x_0}\right\}_{k=0}^{\infty}$. Clearly these functions are linearly independent and form a complete set in $L_2(0,1)$. We apply the classical Gram-Schmidt Orthonormalization procedure to this set. We start from e^{x_0}. Then we take $x_0 e^{x_0}$, then $x_0^2 e^{x_0}$, etc. As a result, we obtain an orthonormal basis in $L_2(0,1)$, which consists of functions $\{P_n(x_0)\, e^{x_0}\}_{n=0}^{\infty} = \{\psi_n(x_0)\}_{n=0}^{\infty}$, where $P_n(x_0)$ is a polynomial of the degree m. Denote $[,]$ the scalar product in $L_2(0,1)$.

Lemma 5.1 (an analog of Lemma 4.1) [7]**.** *We have*

$$a_{nk} = [\psi_k', \psi_n] = \begin{cases} 1 \text{ if } k = n, \\ 0 \text{ if } k < n. \end{cases} \tag{5.1}$$

Let $N \geq 1$ be an integer. Consider the $N \times N$ matrix $M_N = (a_{nk})_{(k,n)=(0,0)}^{(N-1,N-1)}$. Then (5.1) implies that $\det(M_N) = 1$, *which means that there exists the inverse matrix M_N^{-1}.*

5.2 Coefficient inverse scattering problem for Helmholtz equation [7]

While the technique of [7] is applicable to a broad class of CISPs, we focus here on a specific CISP for Helmholtz equation: for brevity.

Similarly with section 2, let $\mathbf{x} = (x, y, z) \in \mathbb{R}^3$. Let the function $c(\mathbf{x})$ satisfy the same conditions (2.7) as in section 2. Also, like in section 2, we assume that $c(\mathbf{x}) \in C^{15}(\mathbb{R}^3)$. The Helmholtz equation for the function $u(\mathbf{x}, k)$ with the radiation condition is and with the source located at $(x_0, 0, -1)$ is

$$\Delta u + k^2 c(\mathbf{x})\, u = -\delta(x - x_0)\, \delta(y, z+1), \tag{5.2}$$

$$\lim_{r \to \infty} \left[r \left(\partial_r u - iku \right) \right] = 0, r = |x|. \tag{5.3}$$

Let a,$d > 0$. We set

$$\Omega = \{x : -a < x, y < a, z \in (0, d)\}. \tag{5.4}$$

Note that the source positions $(x_0, 0, -1) \cap \overline{\Omega} = \varnothing$. We consider Coefficient Inverse Scattering Problem (CISP) with backscattering data and with a fixed value of the wave number $k = k_0$.

Coefficient Inverse Scattering Problem (CISP with backscattering data). *Denote the backscattering side of the rectangular prism Ω as*

$$\Gamma = \{\mathbf{x} : -a < x, y < a, z = 0\}.$$

Determine the unknown coefficient $c(\mathbf{x})$ *for* $\mathbf{x} \in \Omega$, *assuming that the following two functions* $g_0(x,y,x_0), g_1(x,y,x_0)$ *are known for a fixed value of the wavenumber* $k = k_0$*:*

$$u(\mathbf{x},k_0)\mid_\Gamma = g_0(x,y,x_0), \partial_n u(\mathbf{x},k_0)\mid_\Gamma = g_1(x,y,x_0), \forall x_0 \in [0,1]. \tag{5.5}$$

As it was pointed out in section 2.1 with references to [4, 8] and the previous annual report on this grant [23], actually the function u is measured far from the domain of interest Ω. Next, using the data propagation procedure, one can compute functions g_0 and g_1.

Similarly with section 2.2.1 we have the following asymptotic behavior of the function $u(\mathbf{x},x_0,k)$ as $k \to \infty$ [20]

$$u(\mathbf{x},x_0,k) = A(\mathbf{x},x_0)\, e^{ik\tau(\mathbf{x},x_0)} (1 + h(\mathbf{x},x_0,k)), k \to \infty, \forall \mathbf{x} \in \overline{\Omega}, \forall x_0 \in [0,1], \tag{5.6}$$

where $\tau(\mathbf{x},x_0)$ is the travel time between the source $(x_0,0,-1)$ and the point $\mathbf{x}$. The function $h(\mathbf{x},x_0,k)$ is such that $|h((\mathbf{x},x_0,k))| \leq C/k, \forall \mathbf{x} \in \overline{\Omega}$, where $C > 0$ is a certain constant independent on $\mathbf{x}, k$. In (5.6) $A(\mathbf{x},x_0) > 0, \forall \mathbf{x} \in \overline{\Omega}, \forall x_0 \in [0,1]$. It follows from (5.6) that $u(\mathbf{x},x_0,k) \neq 0, \forall \mathbf{x} \in \overline{\Omega}, \forall x_0 \in [0,1]$ for sufficiently large values of k. Hence, assuming that wave number k_0 in (5.5) is sufficiently large, we uniquely define the function $v(\mathbf{x},x_0,k)$

$$v(\mathbf{x},x_0,k_0) = \log u(\mathbf{x},x_0,k_0)$$

as

$$v(\mathbf{x},x_0,k_0) = \log u(\mathbf{x},x_0,k_0) := ik\tau(\mathbf{x},x_0) + \ln A(\mathbf{x},x_0) + \log(1 + h(\mathbf{x},x_0,k_0))$$

$$:= ik\tau(\mathbf{x},x_0) + \ln A(\mathbf{x},x_0) + \sum_{n=1}^{\infty} \frac{(-1)^{n-1}}{n} h^n(\mathbf{x},x_0,k_0), \ \mathbf{x} \in \overline{\Omega}.$$

By (5.2)

$$\Delta v + (\nabla v)^2 = -k_0^2 c(\mathbf{x}), \mathbf{x} \in \overline{\Omega}. \tag{5.7}$$

Differentiating (5.7) with respect to x_0, we obtain

$$\Delta v_{x_0} + 2\nabla v_{x_0} \nabla v = 0. \tag{5.8}$$

We assume that the function $v(\mathbf{x},x_0)$ can be represented as a truncated series,

$$v(x,x_0) = \sum_{k=0}^{N-1} v_k(x)\, \psi_k(x_0), \forall x \in \overline{\Omega}, \forall x_0 \in [0,1], \tag{5.9}$$

where coefficients $v_k(x) \in C^2(\overline{\Omega})$ and $N \geq 1$ is an integer of ones choice. Substituting (5.9) in (5.8), we obtain

$$\sum_{k=0}^{N-1} \Delta v_k(\mathbf{x})\, \psi_k'(x_0) + 2 \sum_{n,m=0}^{N-1} \nabla v_n(\mathbf{x})\, \nabla v_m(\mathbf{x})\, \psi_n'(x_0)\, \psi_m(x_0) = 0. \tag{5.10}$$

Multiply both sides of (5.10) by the function $\psi_s(x_0), s = 0, 1, ..., N-1$ and integrate with respect to $x_0 \in (0,1)$. Denote

$$V(\mathbf{x}) = (v_0(\mathbf{x}), ..., v_{N-1}(\mathbf{x}))^T.$$

We obtain

$$M_N A_0(\mathbf{x}, V) = \widetilde{F}(\nabla V),$$

where M_N is the matrix of Lemma 5.1 and $\widetilde{F}(\nabla V)$ is a vector function, which is quadratic with respect to first derivatives of functions $v_j(\mathbf{x})$. Applying Lemma 5.1 and denoting $P(\nabla V) = M_N^{-1}\widetilde{F}(\nabla V)$, we obtain

$$\Delta V - P(\nabla V) = 0, \tag{5.11}$$

$$V|_\Gamma = p_0(\mathbf{x}), \partial_n V|_\Gamma = p_1(\mathbf{x}), \tag{5.12}$$

where vector functions $p_0(\mathbf{x})$ and $p_1(\mathbf{x})$ are generated by functions $g_0(x, y, x_0)$ and $g_1(x, y, x_0)$ in (5.5). Similarly with (2.10) we also complement the Dirichlet boundary condition in (5.12) as

$$V|_{\partial\Omega\setminus\Gamma} = p_2(\mathbf{x}). \tag{5.13}$$

The problem (5.11)-(5.13) is an ill-posed Cauchy problem for the system (5.11) of coupled quasilinear elliptic equations. To solve this problem, we use the idea of [22] of the PI, where it was applied to an ill-posed problem for a single PDE. In other words, we use the convexification.

While several CWFs can be used for the Laplace operator in (5.11), it seems from our numerical experience that the best way is to use the simplest CWF (2.40),

$$\varphi_\lambda(z) = e^{-2\lambda z}.$$

To do this, we need again write operators Δ and ∇ in the form of finite differences with respect to x, y, as in (2.30)-(6.8). We now refer to definitions and notations of sections 2.3-2.5. We assume that there exists an $N-$D vector function $F(\mathbf{x}) \in H^{2,h}(\Omega_h)$ such that

$$F|_\Gamma = p_0(\mathbf{x}), \partial_n F|_\Gamma = p_1(\mathbf{x}), F|_{\partial\Omega\setminus\Gamma} = p_2(\mathbf{x}).$$

Below in this section 5.2 $p(\mathbf{x})$ are $N-$D vector functions. Hence, we consider the following minimization problem:

Minimization Problem 4. *Minimize the functional*

$$J_\lambda(p) = e^{2\lambda d}\sum_{j,s=1}^{N_h} h^2 \int_{\underline{k}}^{\overline{k}}\int_{-\xi}^{d} \left|\left[\Delta^h(p+F) - P\left(\nabla^h(p+F)\right)\right](x_j, y_s, z, \kappa)\right|^2 \varphi_\lambda(z)\,dz\,d\kappa, \quad p \in \overline{B(R)}, \tag{5.14}$$

where

$$B(R) = \left\{p \in H_0^{2,h}(\Omega_h) : \|p\|_{H^{2,h}(\Omega_h)} < R\right\}$$

and $R > 0$ is an arbitrary number.

Remark 5.1. *Analogs of Theorems 2.1-2.5 are valid for the functional (5.14) [7]. Therefore, we again work with a* ***globally convergent*** *numerical method.*

5.3 Convexification for Electrical Impedance Tomography [13]

Electrical impedance tomography (EIT) is a non invasive and diffusive imaging method to recover the electrical conductivity distribution inside an object of interest by using the DtN map on the boundary. This modality is safe, portable and also has many clinical imaging applications [31]. There is a vast number of research papers discussing EIT, see, e.g.[25, 26, 29, 44, 45] and references cited therein. However, globally convergent numerical methods have not been applied to EIT until the most recent preprint of the PI with coauthors [13]. In addition, while all previous statements of EIT are over determined ones in 3-D, the statement of the PI is non overdetermined.

5.3.1 Statement of the problem

In this section 5.3 $x = (x_1, x_2, ..., x_d) \in \mathbb{R}^d$. To avoid working with singularities and also to simplify the presentation, we model the point source here by a $\delta-$like function instead of the $\delta-$function. Let $\varepsilon > 0$ be a sufficiently small number. Let the source function $f(x)$ be such that

$$f(x) \in C^\infty(\mathbb{R}^n), f(0) \neq 0, f(x) \geq 0, \forall x \in \mathbb{R}^d, \ f(x) = 0 \text{ for } |x| > \varepsilon. \tag{5.15}$$

Let $G \subset \mathbb{R}^n$ be a bounded domain with its boundary $\partial G \in C^1$, $\Omega \subset G$ and $\partial\Omega \cap \partial G = \varnothing$. Let $\overline{x} \in \mathbb{R}^{d-1}$ be a fixed point. For $s \in [0,1]$ denote $x_s = (x_{1s}, \overline{x})$ the position of the point source. Let

$$I = \{x_s = (x_{1s}, \overline{x}) : s \in [0,1]\}$$

be the interval of the straight line $\{x = (x_1, \overline{x}), x_1 \in \mathbb{R}\}$. Let $I_\varepsilon = \{x \in \mathbb{R}^d : dist(x, I) < \varepsilon\}$, where $dist(x, I)$ is the Hausdorff distance between the point x and the set I. We also assume that $I_\varepsilon \subset (G \setminus \overline{\Omega})$, which means that the support of the source function is outside of the domain Ω.

Let the function

$$\sigma(x) \in C^{2+\alpha}(\overline{G}), \sigma(x) = 1 \text{ for } x \in G \setminus \Omega \text{ and } \sigma(x) \geq \sigma_0 = const. > 0. \tag{5.16}$$

Here $\alpha = const. \in (0,1)$ and $C^{k+\alpha}(\overline{G})$ be the Hölder space, where $k \geq 0$ is an integer. Assume first that $\sigma(x)$ is known. For each source position $x_s \in I$ we define the forward boundary value problem for EIT as the problem of finding the function $u(x,s)$ such that

$$\begin{cases} \nabla \cdot (\sigma(x)\nabla u(x,s)) & = -f(x - x_s), & x \in G, \forall x_s \in \overline{I} \\ u(x,s)|_{x \in \partial G} & = 0, & \forall x_s \in \overline{I}. \end{cases} \tag{5.17}$$

It is well known that for each $x_s \in I$ the problem (5.17) has unique solution

$$u(x,s) \in C^{3+\alpha}(\overline{G}), \forall x_s \in \overline{I}, \tag{5.18}$$

see, e.g. [30]. We measure both Dirichlet and Neumann boundary conditions of the function u on a part $\Gamma \subseteq \partial\Omega$ of the boundary $\partial\Omega$,

$$u(x,s)|_{x\in\Gamma,x_s\in\overline{I}} = g_0(x,s) \text{ and } \partial_\nu u(x,s)|_{x\in\Gamma,x_s\in\overline{I}} = g_1(x,s). \tag{5.19}$$

We call the Dirichlet and Neumann boundary data (5.19) "restricted Dirichlet-to-Neumann (DtN) data". Suppose now that the function $\sigma(x)$ is unknown. Then we arrive at the following inverse problem:

Coefficient Inverse Problem (CIP). *Assume that the function $\sigma(x)$ is unknown for $x \in \Omega$ and also that conditions (4.7), (4.8) hold. Also, assume that functions $g_0(x,s)$ and $g_1(x,s)$ in (5.19) are known for all $x \in \Gamma, x_s \in \overline{I}$. Determine the function $\sigma(x)$.*

Note that in this CIP the number d of free variables in the data equals the number of free variables in the unknown coefficient.

In this subsection, we transform the above CIP to an inverse problem for a quasilinear PDE. First, introduce the well known change of variables

$$u_1 = \sqrt{\sigma} u, \tag{5.20}$$

where $u(x,s)$ is the solution of problem (5.17). Then

$$\begin{cases} \Delta u_1(x,s) + a_0(x) u_1(x,s) & = -f(x-x_s), \qquad \forall x_s \in \overline{I}, \\ u_1(x,s)|_{x\in\partial G} & = 0, \qquad \forall x_s \in \overline{I}, \end{cases} \tag{5.21}$$

where

$$a_0(x) = -\frac{\Delta\left(\sqrt{\sigma(x)}\right)}{\sqrt{\sigma(x)}}. \tag{5.22}$$

Recalling that $\sigma = 1$ on $\partial\Omega$, we obtain from (5.19)

$$u_1(x,s)|_{x\in\Gamma,s\in[0,1]} = g_0(x,s) \text{ and } \partial_n u_1(x,s)|_{x\in\Gamma,s\in[0,1]} = g_1(x,s). \tag{5.23}$$

If we would recover the function $a_0(x)$ for $x \in \Omega$ from conditions (5.21), (5.23), then, assuming that 0 is not an eigenvalue of the elliptic operator $\Delta + a_0(x)$ with the Dirichlet boundary condition either on $\partial\Omega$ or on ∂G, we would recover the function $\sigma(x)$ via solving elliptic equation (5.22) either in the domain Ω with the Dirichlet boundary condition $\sigma|_{\partial\Omega} = 1$, or in the domain G with the Dirichlet boundary condition $\sigma|_{\partial G} = 1$. Hence, we focus below on the recovery of the function $a_0(x)$ for $x \in \Omega$ from conditions (5.21), (5.23).

It follows from (4.7), (5.17), (5.20) and the maximum principle for elliptic equations [30] that $u_1(x,s) > 0$ for all $x \in \overline{\Omega}$ and all $s \in [0,1]$. Hence, we can consider the function $v(x,s)$,

$$v(x,s) = \ln u_1(x,s). \tag{5.24}$$

Then $u_1(x,s) = e^{v(x,s)}$ and (5.21) implies that

$$\Delta v(x,s) + (\nabla v(x,s))^2 = -a_0(x), \qquad x \in \Omega, \forall s \in [0,1]. \tag{5.25}$$

Here we use (4.7) and the fact that $I_\varepsilon \subset (G \setminus \overline{\Omega})$. In addition, using (5.23), we obtain

$$v(x,s)|_{x\in\Gamma,s\in[0,1]} = \tilde{g}_0(x,s) \text{ and } \partial_n v(x,s)|_{x\in\Gamma,s\in[0,1]} = \tilde{g}_1(x,s), \tag{5.26}$$

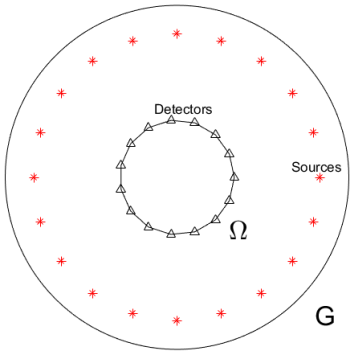

Figure 9: *A schematic diagram of domains G, Ω, sources and detectors in our statement of the problem of electrical impedance tomography*

where

$$\tilde{g}_0(x,s) = \ln g_0(x,s) \text{ and } \tilde{g}_1(x,s) = \frac{g_1(x,s)}{g_0(x,s)}.$$

The problem (5.25), (5.26) is very similar with the above problem (5.7), (5.8). Next, we proceed similarly with the above and obtain the following analog of the problem (5.11), (5.12):

$$\Delta W - Q\left(\nabla W\right) = 0, \tag{5.27}$$

$$W\mid_{\Gamma} = q_0\left(\mathbf{x}\right), \partial_n W\mid_{\Gamma} = q_1\left(\mathbf{x}\right), \tag{5.28}$$

where vector functions $q_0\left(\mathbf{x}\right)$ and $q_1\left(\mathbf{x}\right)$ are known.

Below in this section 5.3 $W\left(\mathbf{x}\right), q\left(\mathbf{x}\right)$ are $N-$D vector functions.

5.3.2 Global strict convexity and numerical results

We have numerically solved EIT for the case when $\Omega \subset \mathbb{R}^2$ is a disk. In all our numerical examples of [13]

$$G = \{x_1^2 + x_2^2 < 5\}, \Omega = \{x_1^2 + x_2^2 \leq 1\}.$$

We measure the data on the whole boundary $\partial\Omega = \Gamma$. The source runs over the circle $C^{(s)} = \{x_1^2 + x_2^2 = 4\}$. In other words, in polar coordinates

$$x_s = (r,s) = (2,s), s = \varphi \in (0, 2\pi), x_s \in C^{(s)}. \tag{5.29}$$

However, when constructing the required orthonormal basis $\{\psi_n(s)\}_{n=0}^{\infty}$, we still have used functions $\{s^n e^s\}_{n=0}^{\infty}$, i.e. we did not impose the periodicity condition on this basis. The source function $f(x)$ in our case is the bump function below:

$$f\left(x - x^{(s)}\right) = \begin{cases} \frac{1}{\varepsilon}\exp\left(-\frac{1}{1-|x-x_s|^2/\varepsilon}\right), \text{ if } \left(x-x_s\right)^2 < \varepsilon, \\ 0, \text{ otherwise.} \end{cases}$$

We have chosen $\varepsilon = 0.01$.

Since in our computations $\partial\Omega = \Gamma = \{r = 1\}$, then we assume that there exists a vector function $F \in H^2(\Omega)$ such that

$$F\mid_{r=1} = q_0(\varphi), F_r\mid_{r=1} = q_1(\varphi), \varphi \in (0, 2\pi).$$

Now, the CWF for the Laplace operator in the domain

$$\Omega_\mu = \{(r, \varphi) : r \in (\mu, 1), \varphi \in (0, 2\pi)\}$$

can be chosen as $e^{2\lambda r}, r \in (\mu, 1)$. We take $\mu = 0.01$ and consider the following minimization problem:

Minimization Problem 5. *Minimize the functional*

$$J_\lambda(q) = \int\limits_{\Omega_\mu} \left[\Delta(q + F) - Q(\nabla(q + F))\right]^2 e^{2\lambda r} r dr d\varphi, q \in \overline{D(R)}, \tag{5.30}$$

where

$$D(R) = \left\{q \in H^2(\Omega_\mu) : q(1, \varphi) = q_r(1, \varphi) = 0, \|q\|_{H^2(\Omega_\mu)} < R\right\},$$

where $R > 0$ is an arbitrary number.

Remark 5.2. *Analogs of Theorems 2.1-2.5 are valid for the functional (5.30) [13]. Therefore, we again work with a* ***globally convergent*** *numerical method.*

We have established by trial and error in our computations that the optimal values of parameters λ and N were

$$\lambda = 1, N = 8.$$

Figures 10 display a sample of our image. One can observe that the case of a moving source allows one to image all three components of abnormalities: locations, shapes and values of the unknown coefficient inside: just as it was anticipated by the PI in item 4 of Abstract.

6 Experimental Phaseless Data [11]

Details of the material of this section can be found in the preprint [11] of the PI with coauthors.

As it was pointed out in Introduction, the topic of Phaseless Coefficient Inverse Scattering Problems (PCISPs) is a minor topic of this project. In a PCISP only the modulus of the complex valued scattered wave field is measured outside of scatterers. Phase is not measured. This topic has applications in imaging of nanostructures and biological cells. The tail functions globally convergent methods of the PI is applied to this problem as an auxiliary tool. Since the work on this topic was mostly supported by the ONR grant N00014-15-1-2330 of the PI (2015-2018) while the current ARO funding was used as a leverage, then the topic of PCISPs is a minor focus of this report. .

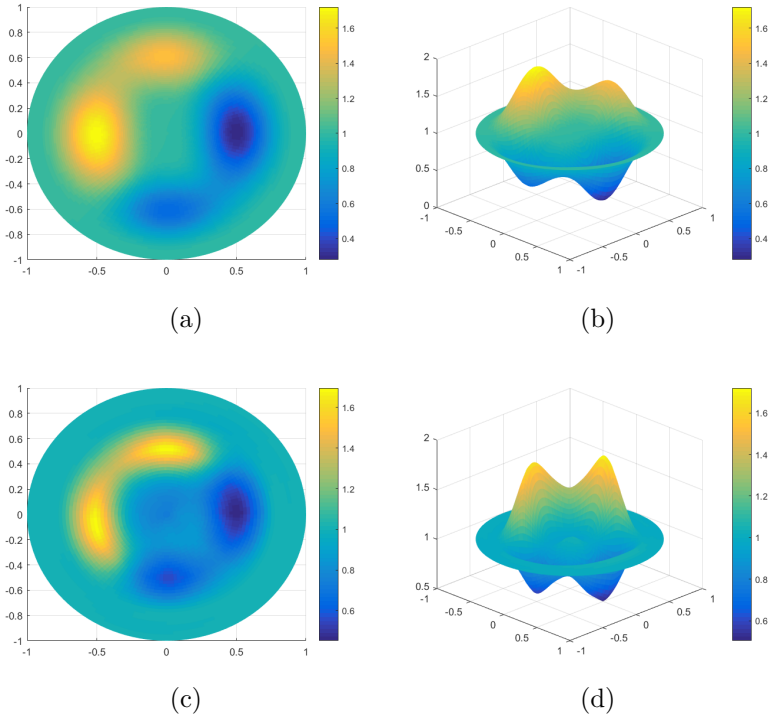

Figure 10: *An image sample for EIT [13] obtained by the globally convergent convexification method of section 5.3, $\lambda = 1, N = 8$. a) True σ. b) 3-D view of true σ. c) Computed 2-D image of σ. d) 3-D presentation of c). In conclusion, one can observe that the case of a moving source allows one to image all three components of abnormalities: locations, shapes and values of the unknown coefficient inside, see item 4 of Abstract.*

(a) *The photograph of our experimental device.*

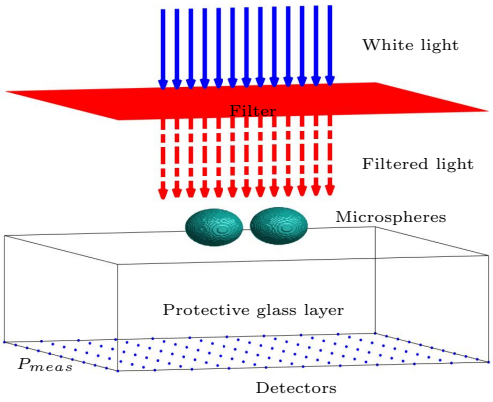

(b) *A schematic diagram of data collection.*

Figure 11: *The data collection setup*

Note that it is the refractive index $n(\mathbf{x})$ which can be measured directly,

$$n(\mathbf{x}) = \sqrt{c(\mathbf{x})}. \tag{6.1}$$

We have imaged one and two microspheres with the following parameters:

$$\text{diameter}=6\mu m, \text{ refractive index } n = 2.15. \tag{6.2}$$

6.1 Measurements

Let Ω be a bounded domain in $\mathbb{R}^3$. Consider positive numbers $b, d_1, d_2 > 0$. Due to our computational arrangements, it is convenient to assume that

$$\Omega = \{\mathbf{x} : |x| < b, |y| < b, -d_1 < z < d_2\}. \tag{6.3}$$

We also set

$$\Gamma = \{\mathbf{x} : |x| < b, |y| < b, z = d_2\} \subset \partial\Omega. \tag{6.4}$$

Let the number $R > d_2$. Consider the plane P,

$$P = \{z = R\}.$$

We define the square $P_{\text{meas}} \subset P$ as

$$P_{\text{meas}} = \{\mathbf{x} : |x| < b, |y| < b, z = R\}. \tag{6.5}$$

Hence, P_{meas} is part of the plane $\{z = R\}$ and measurements of the intensity $|u_{\text{sc}}(\mathbf{x}, k)|^2$ are performed on P_{meas}. Here R is the distance from the origin to the measurement plane and $4b^2$ is the area of that square. Since $R > d_2$, then $\overline{\Omega} \cap P_{\text{meas}} = \varnothing$.

The idea is to use the chip from a cell phone to get the intensity data. This idea is actually taken from [49] and a number of other publications of this research group. However, unlike [49], we go beyond just data collection. In fact, our goal it to reconstruct both locations and refractive indices of microspheres. We send the white light as a plane wave and measure the intensity on a part P_{meas} of a plane whose distance from the microspheres is between 330 μm, see Figures 10. However, to have the varying wave number k, we use several light filters, which give us intensity on six (6) different wavelengths (in microns):

$$\lambda = 0.420, 0.473, 0.525, 0.580, 0.620, 0.671(\mu m). \tag{6.6}$$

In fact, (6.6) correspond to the following dimensionless wave numbers:

$$k = 93.6, 101.3, 108.3, 119.7, 132.8, 149.5. \tag{6.7}$$

However, we have discovered that the data have a reasonable amount of noise for only two values of k in (6.7), $k = 108.3$ and $k = 119.7$. Hence, to obtain the data for $k \in (108.3, 119.7)$, we linearly interpolate our data between these two values of k. Thus, we set below

$$\left[\underline{k}, \overline{k}\right] = [108.3, 119.7]. \tag{6.8}$$

Let $u(\mathbf{x}, k)$ be the solution of the problem (2.4)-(2.6) for the Helmholtz equation with the incident plane wave as in (4.24),

$$u_i = e^{ikz}.$$

Denote $u_{\text{sc}} = u - u_i$ the scattered wave.

Phaseless Coefficient Inverse Scattering Problem (PCISP). *Assume that the function* $f(\mathbf{x}, k)$,

$$f(\mathbf{x}, k) = |u(\mathbf{x}, k)|^2, \quad \mathbf{x} \in P_{\text{meas}}, k \in [\underline{k}, \overline{k}] \tag{6.9}$$

is known. Determine the function $n(x)$ *for* $x \in \Omega$.

Remark 6.1. *We work here with the Helmholtz equation model (2.4)-(2.6), although the full Maxwell's system is a more accurate model to describe the propagation of the electromagnetic waves. Nevertheless, in our numerical study, the Helmholtz equation model shows reasonable agreements with the experimental data. We justify this numerically in Appendix of our work [11].*

6.2 An important theoretical result involving Riemannian geometry

We have we have for $k \in [\underline{k}, \overline{k}]$ and $\mathbf{x} \in P_{\text{meas}}$:

$$|u|^2 = 1 + e^{ikz}\overline{u_{\text{sc}}} + e^{-ikz}u_{\text{sc}} + |u_{\text{sc}}|^2, \tag{6.10}$$

where P_{meas} is defined in (6.5). To derive the reconstruction formula for PCISP, we need to drop the term $|u_{\text{sc}}|^2$ here.

It follows from the Lippmann-Schwinger equation

$$u_{\text{sc}}(\mathbf{x},k) = k^2 \int\limits_{\Omega} \frac{\exp(ik|\mathbf{x}-\boldsymbol{\xi}|)}{4\pi|\mathbf{x}-\boldsymbol{\xi}|} \left(n^2(\boldsymbol{\xi})-1\right) u(\boldsymbol{\xi},k) d\boldsymbol{\xi},\ \mathbf{x} \in P_{\text{meas}}. \tag{6.11}$$

We can see from (6.11) that $|u_{\text{sc}}(\mathbf{x},k)|$ grows at the order of $O(k^2)$ as $k \to \infty$. The goal of Theorem 6.1 is to decrease this growth to $O(k)$.

To analytically derive the desired upper estimate, we impose the following assumption:

$$\max_{\mathbf{x} \in \overline{\Omega'}} \left| \int_{\Gamma(\mathbf{x},a)} n\left(\boldsymbol{\xi}\right) d\sigma - \int_{L(\mathbf{x},a)} n\left(\boldsymbol{\xi}\right) d\sigma \right| \ll 1 \tag{6.12}$$

where $\boldsymbol{\xi} = (\xi_1, \xi_2, \xi_3)$,

$$\Omega' = \{\mathbf{x} : n(\mathbf{x}) > 1\} \subset \Omega \tag{6.13}$$

and $L\left(\mathbf{x},a\right)$ is a straight line connecting the point $\mathbf{x}$ with the plane P_a in (2.11), which is orthogonal to the $z-$axis. Intuitively this assumption might be justified by the fact that the domain Ω' is actually the one occupied by microspheres to be imaged. So, since microspheres are small, then the domain Ω' is also small. To justify our assumption (6.12) further, we note that

$$\Gamma\left(\mathbf{x},a\right) = L\left(\mathbf{x},a\right), \quad \mathbf{x} \in \left\{(x,y,z) : -a < z < -d_1\right\}.$$

Thus, by assumption (6.12) we replace, for $\mathbf{x} \in \overline{\Omega'}$, the integral of $n\left(\boldsymbol{\xi}\right)$ over the geodesic line $\Gamma\left(\mathbf{x},a\right)$ with the integral of $n\left(\boldsymbol{\xi}\right)$ over the straight line $L\left(\mathbf{x},a\right)$, i.e. we set

$$\int_{\Gamma(\mathbf{x},a)} n\left(\boldsymbol{\xi}\right) d\sigma = \int_{L(\mathbf{x},a)} n\left(\boldsymbol{\xi}\right) d\sigma = \int_{-a}^{z} n(\boldsymbol{\xi}) d\sigma, \quad \forall \mathbf{x} \in \overline{\Omega'} \tag{6.14}$$

Since by (6.5), $\mathbf{x} = (x,y,R)$ for $\mathbf{x} \in P_{\text{meas}}$, assuming that $R \gg \max\left(b,1\right)$, we easily obtain from (6.11) the following analog of the well-known formula for the far field approximation:

$$u_{\text{sc}}(\mathbf{x},k) = \frac{k^2}{4\pi R} e^{ikR} \int_{\Omega'} e^{-ik\xi_3} \left(n^2(\boldsymbol{\xi})-1\right) u(\boldsymbol{\xi},k) d\boldsymbol{\xi}, \quad \mathbf{x} \in P_{\text{meas}}. \tag{6.15}$$

We use in (6.14) and (6.15) "=" instead of "$\approx$" only for the convenience of the *a priori* bound established in Theorem 6.1 below. Now, $n(\boldsymbol{\xi}) = 1$ in $\Omega \setminus \Omega'$. Hence, one can replace in (6.15) Ω' with Ω. Hence, (6.15) is equivalent with

$$u_{\text{sc}}(\mathbf{x},k) = \frac{k^2}{4\pi R} e^{ikR} \int_{\Omega} e^{-ik\xi_3} \left(n^2(\boldsymbol{\xi})-1\right) u(\boldsymbol{\xi},k) d\boldsymbol{\xi}, \quad \mathbf{x} \in P_{\text{meas}}. \tag{6.16}$$

Theorem 6.1. *Suppose that assumption (6.14) holds true. Then the function* $u_{\text{sc}}(x,k)$ *given in* (6.15) *satisfies the following inequality*

$$|u_{\text{sc}}(\mathbf{x},k)| \leq C \frac{k}{4\pi R} \left(1 + O\left(1/k\right)\right), \quad \mathbf{x} \in P_{\text{meas}}, k \to \infty, \tag{6.17}$$

where the number $C > 0$ depends only on the domain Ω and functions $A(\mathbf{x})$ and $n(\mathbf{x})$ for $x \in \Omega$.

Hence, by (6.17)

$$|u_{\text{sc}}(\mathbf{x}, k)|^2 \leq C \left(\frac{k}{4\pi R}\right)^2 (1 + O(1/k)), \ \mathbf{x} \in P_{\text{meas}}, \quad k \to \infty.$$

Using our specific values of parameters $R = 49.5, k \in [108.3, 119.7]$ which we have used in experiments and numerically generating the function $|u_{\text{sc}}(\mathbf{x}, k)|^2$, we came to the conclusion in [11] that the number

$$\left(\frac{k}{4\pi R}\right)^2$$

estimates $|u_{\text{sc}}(\mathbf{x}, k)|^2$ quite accurately from the above, and indeed, for our values of parameters

$$|u_{\text{sc}}(\mathbf{x}, k)|^2 << 1. \tag{6.18}$$

6.3 Inversion formula

We drop below the term $s(\mathbf{x}, k) = O(1/k)$ in the asymptotic expansion (2.12).

Theorem 6.1 and (6.18) allow us to drop the small term $|u_{\text{sc}}|^2$ in (6.10) and obtain:

$$|u(\mathbf{x}, k)|^2 = 1 + 2\,\text{Re}(e^{-ikz} u_{\text{sc}}), \quad \mathbf{x} \in P_{\text{meas}}, k \in [\underline{k}, \overline{k}]. \tag{6.19}$$

Using (6.19) and (2.12), we obtain

$$|u(\mathbf{x}, k)|^2 = -1 + 2A(\mathbf{x}) \cos(k(\tau(\mathbf{x}) - a - z)) \tag{6.20}$$

for all $k \in [\underline{k}, \overline{k}]$. Using (6.9), we choose the *largest value* of $k = \overline{k}$ available in our experimental data, to approximate the function $A(\mathbf{x})$ as

$$A(\mathbf{x}) = |u(\mathbf{x}, \overline{k})| = \sqrt{f(\mathbf{x}, \overline{k})}, \quad \mathbf{x} \in P_{\text{meas}}. \tag{6.21}$$

Next, using (6.20) and (6.21), we obtain

$$f(\mathbf{x}, k) = -1 + 2\sqrt{f(\mathbf{x}, \overline{k})} \cos[k(\tau(\mathbf{x}) - a - z)], \quad \mathbf{x} \in P_{\text{meas}}, k \in [\underline{k}, \overline{k}]. \tag{6.22}$$

Hence,

$$\tau(\mathbf{x}) - a = \frac{1}{k} \arccos\left(\frac{f(\mathbf{x}, k) + 1}{2\sqrt{f(\mathbf{x}, \overline{k})}}\right) + R + \frac{2\pi m}{k}, \quad \mathbf{x} \in P_{\text{meas}}, k \in [\underline{k}, \overline{k}] \tag{6.23}$$

for some integer $m = m(\mathbf{x}, k)$. Plugging this function $\tau(\mathbf{x}) - a$ into (2.12), using (6.20) and (6.21) and noting that $e^{2im\pi} = 1$, we obtain the following *inversion formula*

$$u(\mathbf{x}, k) = \sqrt{f(\mathbf{x}, \overline{k})} \exp\left[\mathrm{i} \arccos\left(\frac{f(\mathbf{x}, k) + 1}{2\sqrt{f(\mathbf{x}, \overline{k})}} \right) + \mathrm{i}kR \right], \ \mathbf{x} \in P_{\text{meas}}, k \in [\underline{k}, \overline{k}]. \quad (6.24)$$

Due to the approximate nature of formula (6.22), the right hand side of (6.23) depends on k. However, k runs only along a narrow interval $k \in [\underline{k}, \overline{k}]$ in (6.23), (6.24), and this interval is given in (6.8). Hence, the right hand side of (6.23) does not change much when $k \in [\underline{k}, \overline{k}]$ changes.

Since formulae (6.23) and (6.24) are approximate ones and also since the data $f(\mathbf{x}, k)$ contain noise, then the argument of the function arccos in (6.23) and (6.24) might exceed 1. In particular, this is true when setting in (6.24) $k := \overline{k}$. Thus, in all cases whenever the argument of the function arccos in (6.23) exceeds 1, we set in our computations this arccos to be equal to zero in (6.23), (6.24). We have noticed in our computations that there are many points at which the argument of arccos in (6.23) is less than 1.

Finally, the key point is that, regardless on the approximate nature of formula (6.24), our numerical results show that it provides an accurate approximation for the function $u(\mathbf{x}, k)$, see below.

6.4 Results of imaging from phaseless experimental data

We solve PCISP in three steps:

1. **Step 1**. Use the inversion formula (6.24). Recover the function $u(\mathbf{x}, k)$ on the measurement site $\mathbf{x} \in P_{\text{meas}}, k \in [\underline{k}, \overline{k}]$. This way we obtain the data for the Phased Coefficient Inverse Scattering Problem.

2. **Step 2**. Use the data propagation procedure of [8] to back propagate the data from P_{meas} to the part Γ in (6.4) of the boundary of the domain of interest Ω.

3. **Step 3**. Use the tail functions globally convergent numerical method [2] to find the target unknown coefficient $c(\mathbf{x})$ for $\mathbf{x} \in \Omega$ via the solution of the Phased Coefficient Inverse Scattering Problem with the data at Γ.

We have decided in [11] to verify our reconstructions from experimental data by reconstructions from computationally simulated data. Thus, we have solved the forward problem (4.24), (2.4)-(2.6) for exactly the same microspheres as ones in (6.2). Other parameters were also kept the same as ones in the experiment. Next, we have compared reconstruction results from experimental data with reconstruction results from computationally simulated data.

6.4.1 One microsphere

First, we verify the accuracy of the reconstruction formula (6.24) for computationally simulated data. Figures 6 displays these results. The relative error in the real part of $u\left(\mathbf{x},\overline{k}\right)$ does not exceed 6% and the error in the imaginary part does not exceed 4%.

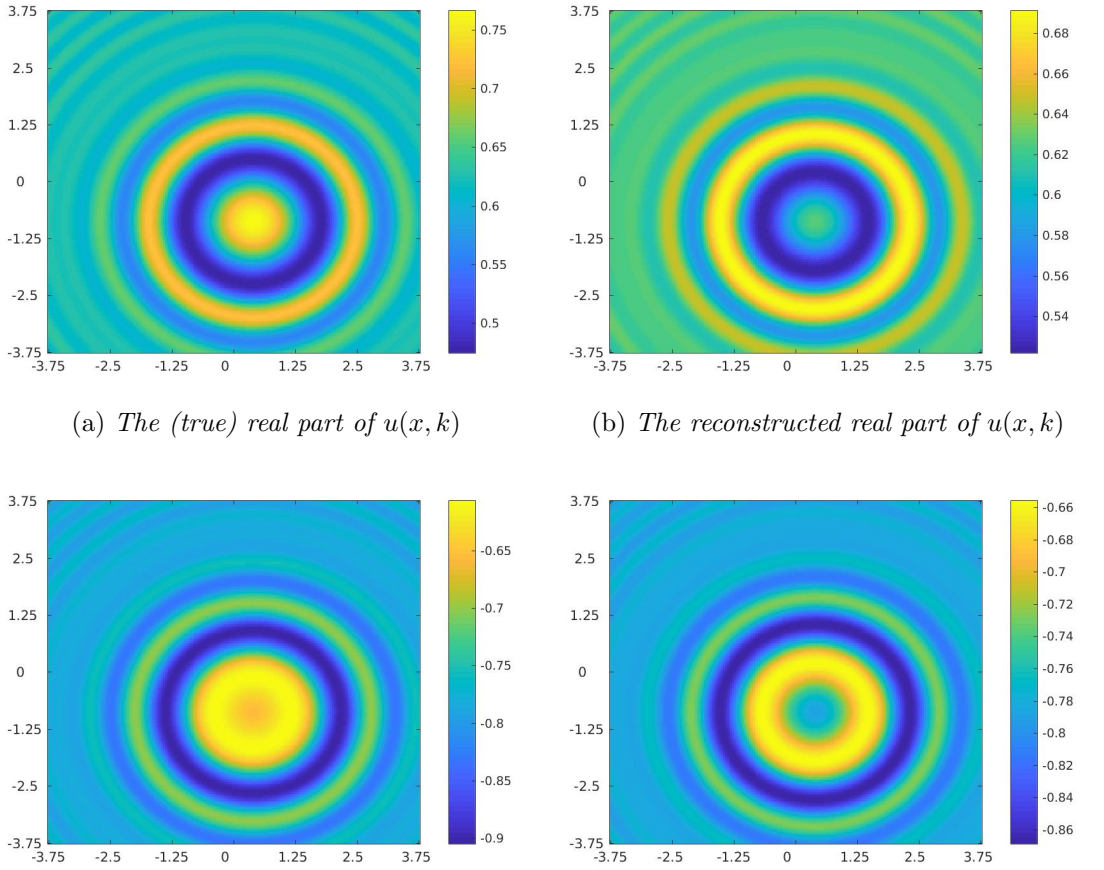

(a) *The (true) real part of* $u(x,k)$ (b) *The reconstructed real part of* $u(x,k)$

(c) *The (true) imaginary part of* $u(x,k)$ (d) *The reconstructed imaginary part of* $u(x,k)$

Figure 12: *The reconstruction of the complex valued function* $u\left(\mathbf{x},\overline{k}\right)$ *with* $\overline{k}=119.7$ *using the inversion formula (6.24). Computationally simulated data are used. The relative error between the true real part and the reconstructed real part of* $u\left(\mathbf{x},\overline{k}\right)$ *is 6%, and this error is 4% for the imaginary parts. Thus, the reconstruction formula (6.24) provides a quite accurate reconstruction of the function* $u(x,k)$ *for* $\mathbf{x}\in P_{\text{meas}}$.

6.4.2 Two microspheres

We now consider the case of two microspheres.

Table 6: One microsphere. True and computed values of the refractive indices in the reconstructed microsphere.

Data	True n (microsphere)	n_{comp} (microsphere)	Relative error
Experimental	2.15	2.043	4.98%
Simulated	2.15	2.040	5.12%

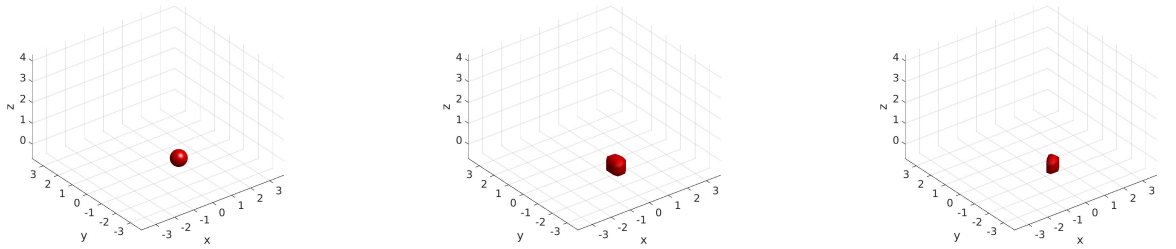

(a) *True image*

(b) *Image computed from simulated data.*

(c) *Image computed from experimental data.*

Figure 13: *True and computed images of the microsphere involved in the experiment. One can observe that the location of the unknown microsphere is imaged with a very good accuracy in both cases. A similarity between (b) and (c) can also be observed. Refractive indices are also computed very accurately for both computationally simulated and experimental data, see Table 6.*

Table 7: Two microspheres. True and computed values of the refractive indices in the reconstructed microsphere.

Data	(true) n (microsphere)	n_{comp} (microsphere)	Relative error
Experimental	2.15	2.04 (in both microspheres)	5.12%
Simulated	2.15	2.04 (in both microspheres)	5.12%

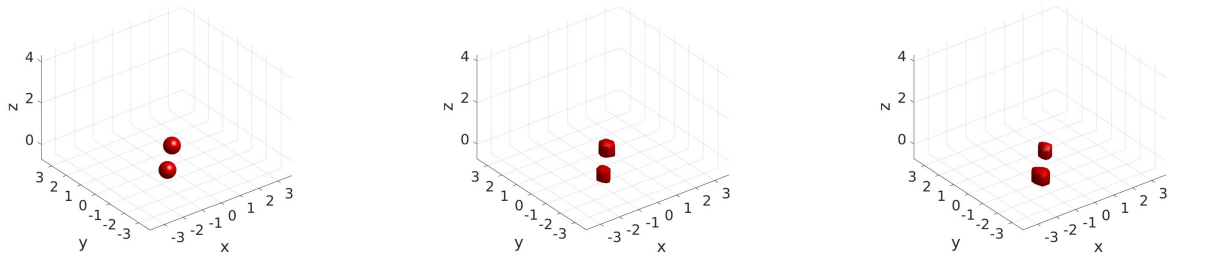

(a) *True image*

(b) *Image computed from simulated data*

(c) *Image computed from experimental data*

Figure 14: *Correct and computed images of two microspheres involved in the experiment. One can observe that the locations of the unknown microspheres are imaged with a very good accuracy in both cases. A close similarity between (b) and (c) can also be observed. Refractive indices are also computed very accurately for both computationally simulated and experimental data, see Table 7.*

Figure 15: *A photograph of the PI with Golden Medal awarded for his Distinguished Impact in Mathematics. The medal was awarded by Sobolev Institute of Mathematics in 2017.*

6.5 Conclusions

It is clear from subsections 6.4.1, 6.4.2 that results for computationally simulated data are practically the same as ones for experimental data. This tells one that our modeling is a quite accurate one. Also, one can observe that we image locations and refractive indices of microspheres with a very good accuracy: the relative error does not exceed 5.12%

7 Prestigious Award

In August 2017 Sobolev Institute of Mathematics has awarded the PI Golden Medal for "Distinguished Impact in Mathematics". This is a life time achievement of the PI.

Other awardees of this Golden Medal are World famous mathematicians, including one Fields Laureate (E.I. Zelmanov).

8 Presentations

The PI has presented above described results on a number of professional meetings. The title of all presentations was about the same, i.e. "Phaseless Inverse Scattering and Global Convergence for Coefficient Inverse Problems". Those meetings were:

1. Conference at Sobolev Institute of Mathematics, Novosibirsk, Russia, August 2017.
2. Conference in Moscow Physics and Technical University, December 2017.

3. Seminar on Inverse and Ill-Posed Problems at Moscow State University, December 2017.

4. Seminar at Gent University (Gent, Belgium), March 2018.

5. International Conference on Mathematics and Statistics (ICOMAS 2018), University of Memphis, May 2018.

6. 9th International Conference "Inverse Problems: Modeling and Simulations", Malta, May 2018.

9 Publications

Total nine (9) papers [1]-[9] were published during the reportage period, and five papers (5) [10]-[14] were submitted in this period.

Total twenty two (22) papers [1]-[22] were published/submitted during the period of this funding June 1, 2015-May 31, 2018. All these papers are in refereed journala and in all papers the support of this grant is acknowledged.

In particular, five (5) joint publications of the PI with ARL engineers Drs. Anders Sullivan and Lam Nguyen are [6, 15, 32, 34, 35], and one joint paper [14] is submitted.

References

[1] M.V. Klibanov and A.E. Kolesov, Convexification of a 3-D coefficient inverse scattering problem, *Computers and Mathematics with Applications*, available online of this journal, https://doi.org/10.1016/j.camwa.2018.03.016, 2018.

[2] M. V. Klibanov, D.-L. Nguyen, L. H. Nguyen, and H. Liu, A globally convergent numerical method for a 3D coefficient inverse problem with a single measurement of multifrequency data, *Inverse Problems and Imaging,* 12, 493-523, 2018.

[3] M.V. Klibanov and V.G. Romanov, Uniqueness of a 3-D coefficient inverse scattering problem without the phase information, *Inverse Problems,* 33, 095007, 2017.

[4] D.-L. Nguyen, M. V. Klibanov, L.H. Nguyen, A. E. Kolesov, M. A. Fiddy and H. Liu, Numerical solution for a coefficient inverse problem with multi-frequency experimental raw data by a globally convergent algorithm, *J. Computational Physics*, 345, 17-32, 2017.

[5] A. E. Kolesov, M. V. Klibanov, L. H. Nguyen, D.-L. Nguyen, and N. T. Thanh, Single measurement experimental data for an inverse medium problem inverted by a multi-frequency globally convergent numerical method, *Applied Numerical Mathematics*, 120, 176-196, 2017.

[6] M.V. Klibanov, A.E. Kolesov, L. Nguyen and A. Sullivan, Globally strictly convex cost functional for a 1-D inverse medium scattering problem with experimental data, *SIAM J. Applied Mathematics,* 77 1733-1755, 2017.

[7] M. V. Klibanov, Convexification of restricted Dirichlet-to-Neumann map, *J. Inverse and Ill-Posed Problems*, 25, 669-685, 2017.

[8] D.-L. Nguyen, M. V. Klibanov, L.H. Nguyen and M.A. Fiddy, Imaging of buried objects from multi-frequency experimental data using a globally convergent inversion method, *Journal of Inverse and Ill-Posed Problems*, published online of this journal, DOI: 10.1515/jiip-2017-0047, 2017.

[9] M.V. Klibanov, A phaseless inverse scattering problem for the 3-D Helmholtz equation, *Inverse Problems and Imaging*, 11, 263-276, 2017.

[10] M.V. Klibanov, D.-L. Nguyen and L. H. Nguyen, A coefficient inverse problem with a single measurement of phaseless scattering data, submitted for publication, *www.arxiv.org:* 1710.04804, submitted for publication, 2018.

[11] M.V. Klibanov, N.A. Koshev, D.-L. Nguyen, L. H. Nguyen, A. Brettin and V.N. Astratov, A numerical method to solve a phaseless coefficient inverse problem from a single measurement of experimental data, submitted for publication, available on *www.arxiv.org*: 1803.01374, submitted for publication, 2018.

[12] M.V. Klibanov, A.E. Kolesov and D.-L. Nguyen, Convexification method for a coefficient inverse problem and its performance for experimental backscatter data for buried targets, available on *www.arxiv.org*: 1850.07618, 2018, submitted for publication.

[13] M. V. Klibanov, J. Li and W. Zhang, Electrical impedance tomography with restricted Dirichlet-to-Neumann map data, available *www.arxiv.org*: 1803.11193, 2018, submitted for publication.

[14] M.V. Klibanov, A.E. Kolesov, A. Sullivan and L. Nguyen, A new version of the convexification method for a 1-D coefficient inverse problem with experimental data, available on *www.arxiv.org*: 1805.06025, 2018, submitted for publication.

[15] M.V. Klibanov, L.H. Nguyen, A. Sullivan and L. Nguyen, A globally convergent numerical method for a 1-d inverse medium problem with experimental data, *Inverse Problems and Imaging*, 10, 1057-1085, 2016.

[16] M.V. Klibanov, L.H. Nguyen and K. Pan, Nanostructures imaging via numerical solution of a 3-D inverse scattering problem without the phase information, *Applied Numerical Mathematics*, 110, 190-203, 2016.

[17] A.B. Bakushinskii, M.V. Klibanov and N.A. Koshev, Carleman weight functions for a globally convergent numerical method for ill-posed Cauchy problems for some quasilinear PDEs, *Nonlinear Analysis: Real World Applications*, 34, 201-224, 2017.

[18] M.V. Klibanov, N.A. Koshev, J. Li and A.G. Yagola, Numerical solution of an ill-posed Cauchy problem for a quasilinear parabolic equation using a Carleman weight function, *J. Inverse and Ill-Posed Problems,* 24, 761-776, 2016.

[19] M.V. Klibanov and V.G. Romanov, The first solution of a long standing problem: Reconstruction formula for a 3-d phaseless inverse scattering problem for the Schrödinger equation, *J. Inverse and Ill-Posed Problems*, 23, 415-428, 2015.

[20] M.V. Klibanov and V.G. Romanov, Reconstruction procedures for two inverse scattering problems without the phase information, *SIAM J. Appl. Math.*, 76, 178-196, 2016.

[21] M.V. Klibanov and V.G. Romanov, Two reconstruction procedures for a 3-D phaseless inverse scattering problem for the generalized Helmholtz equation, *Inverse Problems*, 32, 015005, 2016.

[22] M.V. Klibanov, Carleman weight functions for solving ill-posed Cauchy problems for quasilinear PDEs, *Inverse Problems*, 31, 125007, 2015.

[23] M.V. Klibanov, Globally Convergent Inverse Algorithms via Carleman Weight Functions: Theory, Numerical Studies and Experimental Verifications, *Annual report for the ARO grant W911NF-15-1-0233*, 2017.

[24] L. Beilina and M.V. Klibanov, *Approximate Global Convergence and Adaptivity for Coefficient Inverse Problems*, Springer, New York, 2012.

[25] L. Borcea. *Electrical impedance tomography,* Inverse Problems, 18, pp. R99-R136, 2002.

[26] A. P. Calderon. *On an inverse boundary value problem,* Seminar on Numerical Analysis and its Applications to Continuum Physics (Rio de Janeiro, 1980), Soc. Brasil. Mat., Rio de Janeiro, pp. 65–73.

[27] K. Chadan and P. C. Sabatier, *Inverse Problems in Quantum Scattering Theory*, Springer, New York, 1977.

[28] H. T. Chuah, K. Y. Lee, and T. W. Lau. Dielectric constants of rubber and oil palm leaf samples at x-band, *IEEE Transactions on Geoscience and Remote Sensing*, 33, 221-223, 1995.

[29] M. Dodd and J. Mueller, *A real-time d-bar algorithm for 2-d electrical impedance tomography data, Inverse Problems and Imaging*, 8,1013-1031, 2014.

[30] D. Gilbarg and N.S. Trudinger, *Elliptic Partial Differential Equations of Second Order*, Springer, New York, 1984.

[31] D. Holder. *Electrical Impedance Tomography: Methods, History and Applications*, Institute of Physics, Bristol, 2005.

[32] A.L. Karchevsky, M.V. Klibanov, N. Pantong, L. Nguyen and A. Sullivan, The Krein method and the globally convergent method for experimental data, *Applied Numerical Mathematics*, 74, 111-127, 2013.

[33] M. V. Klibanov A. V. Kuzhuget. Global convergence for a 1-d inverse problem with application to imaging of land mines, *Applicable Analysis*, 89, 125-157, 2010.

[34] A.V. Kuzhuget, L. Beilina, M.V. Klibanov, A. Sullivan, L. Nguyen and M.A. Fiddy, Blind backscattering experimental data collected in the field and an approximately globally convergent inverse algorithm, *Inverse Problems*, 28, 095007, 2012.

[35] A.V. Kuzhuget, L. Beilina, M.V. Klibanov, A. Sullivan, L. Nguyen and M.A. Fiddy, Quantitative image recovery from measured blind backscattered data using a globally convergent inverse method, *IEEE Transaction for Geoscience and Remote Sensing*, 51, 2937–2948, 2013.

[36] M.V. Klibanov, Carleman estimates for global uniqueness, stability and numerical methods for coefficient inverse problems, *J. Inverse and Ill-Posed Problems*, 21, 477-560, 2013.

[37] M.V. Klibanov, Carleman estimates for the regularization of ill-posed Cauchy problems, *Applied Numerical Mathematics*, 94, 46-740, 2015.

[38] M.V. Klibanov, Phaseless inverse scattering problems in three dimensions, *SIAM J. Appl. Math.*, 74, 392-410, 2014.

[39] M.V. Klibanov, On the first solution of a long standing problem: Uniqueness of the phaseless quantum inverse scattering problem in 3-d, *Applied Mathematics Letters*, 37, 82-85, 2014.

[40] M.V. Klibanov, Uniqueness of two phaseless non-overdetermined inverse acoustics problems in 3-d, *Applicable Analysis*, 93, 1135-1149, 2014.

[41] L. Nguyen, D. Wong, M. Ressler, F. Koenig, B. Stanton, G. Smith, J. Sichina, and K. Kappra, Obstacle avoidance and concealed target detection using the Army Research Lab ultra-wideband synchronous impulse reconstruction (UWB SIRE) forward imaging radar, *SPIE Proceedings*, 2007, p. 65530H.

[42] V.G. Romanov, *Inverse Problems of Mathematical Physics*, VNU Press, Utrecht, 1986.

[43] V.G. Romanov, Inverse problems for differential equations with memory, *Eurasian J. of Mathematical and Computer Applications*, 2, issue 4, pp. 51-80, 2014.

[44] S. J. Hamilton, M. Lassas, and S. Siltanen. A direct reconstruction method for anisotropic electrical impedance tomography, *Inverse Problems*, 30 (2014), pp. 075007.

[45] S. J. Hamilton, J. M. Reyes, S. Siltanen, and X. Zhang, *A hybrid segmentation and d-bar method for electrical impedance tomography, SIAM Journal on Imaging Sciences*, 9, 770–793, 2016.

[46] M. Soumekh, *Synthetic Aperture Radar Signal Processing with MATLAB Algorithms*, John Wiley& Sons, New York, 1999.

[47] http://www.clippercontrols.com/pages/Dielectric-Constant-Values.html.

[48] A.N. Tikhonov, A.V. Goncharsky, V.V. Stepanov and A.G. Yagola, *Numerical Methods for the Solution of Ill-Posed Problems*, Kluwer, London, 1995.

[49] D. Tseng, O. Mudanyali, C. Oztoprak, S. O. Isikman, I. Sencan, O. Yaglideresa and A. Ozcan, Lensfree microscopy on a cellphone, *Lab Chip*, 10, 1787–1792, 2010.

[50] B.R. Vainberg, On the short wave asymptotic behaviour of solutions of stationary problems and the asymptotic behaviour at $t \to \infty$ of solutions of non-stationary problems, *Russian Mathematical Surveys,* 30:2, pp. 1-58, 1975.